

AperTO - Archivio Istituzionale Open Access dell'Università di Torino

**Thermosetting Polyurethane Resins as Low-Cost, Easily Scalable, and Effective Oxygen and Moisture Barriers for Perovskite Solar Cells**

**This is a pre print version of the following article:**

*Original Citation:*

*Availability:*

This version is available <http://hdl.handle.net/2318/1766497> since 2021-01-29T15:36:39Z

*Published version:*

DOI:10.1021/acsami.0c17652

*Terms of use:*

Open Access

Anyone can freely access the full text of works made available as "Open Access". Works made available under a Creative Commons license can be used according to the terms and conditions of said license. Use of all other works requires consent of the right holder (author or publisher) if not exempted from copyright protection by the applicable law.

(Article begins on next page)

# Thermosetting polyurethanes resins as low-cost, easily scalable and effective oxygen and moisture barriers for Perovskite Solar Cells

*Matteo Bonomo, Babak Taheri, Luca Bonandini, Sergio Castro-Hermosa, Thomas M. Brown, Marco Zanetti, Alberto Menozzi, Claudia Barolo\* and Francesca Brunetti\**

Dr. M. Bonomo, Prof. M. Zanetti and Prof. C. Barolo

Department of Chemistry and NIS Interdepartmental Centre, University of Turin, Via Pietro Giuria 7, 10125 Turin, Italy

Dr. B. Taheri, Dr. S. Castro-Hermosa, Prof. T.M. Brown and Prof. F. Brunetti

CHOSE (Centre for Hybrid and Organic Solar Energy), Department of Electronic Engineering, University of Rome Tor Vergata, Via del Politecnico 1, 00133 Rome, Italy

L. Bonandini and A. Menozzi

S.E. Special Engines S.r.l., Strada del Cascinotto, 163, 10156 Torino, Italy

Prof. M. Zanetti and Prof. C. Barolo

ICxT Interdepartmental Centre, Università degli Studi di Torino, Lungo Dora Siena 100, 10153 Torino, Italy

KEYWORDS. Perovskite Solar Cells, Polyurethanes, Encapsulation, Oxygen Barrier, Water-Vapor Barrier.

**ABSTRACT.** Long-term stability of Perovskite Solar Cells (PSCs) is one of the main issues to be solved for a forthcoming commercialization of this technology. In this work, thermosetting polyurethane-based resins (PU) are proposed as effective encapsulants for Perovskite Solar Cells to prevent degradation caused by both moisture and oxygen. Application consists in a direct drop-cast of precursor mixture onto the back of the device followed by in-situ polymerization, avoiding the use of other adhesives. PU are cost effective, lightweight, thermal and light-stable materials whose mechanical, chemical and physical properties can be easily tuned by thoughtful choice of their precursor. Encapsulated PSCs show extremely good stability when stored under ambient light (maximum 1000 lux) controlled humidity (28-65%) and temperature (18-30 °C) by retaining 94% of the initial power conversion efficiency after 2500 hours (4 months) whereas control devices lose 90% of their performance after 500 hours ( $T_{80} = 37$  h); once stored according to ISOS-D-1 PU-protected devices showed  $T_{80} > 1200$  h.. Encapsulated devices are stable even when immersed in pure water. Throughout this paper, it is demonstrated the use of PU as promising solution processed encapsulant materials for PSC, which can be a cost-effective route for future industrialization of this technology.

## **1. Introduction**

In the last years, Perovskite Solar Cells (PSCs) attracted huge attention from scientists involved in the photovoltaic field due to their impressive solar-to-electrical energy conversion efficiency.<sup>1</sup> Indeed, PSC remarkably outperformed other recent technologies (known as emerging photovoltaics), such as Dye-Sensitized Solar Cells (DSSC)<sup>2</sup> and Organic Photovoltaics (OPVs),<sup>3</sup> and have recently approached the efficiency of classical PV, e.g. Si-based devices. Additionally, PSCs can be effectively employed in different light condition (from full Sun to indoor illumination<sup>4</sup>) and in a plethora of different applications.<sup>5</sup>

Unfortunately, up to now, PSCs heavily suffer from instability due to intrinsic degradation<sup>6</sup> of the materials used for the realization of the device and to extrinsic degradation related to the interaction with the environment.<sup>7</sup> Indeed, both oxygen and moisture are external agents which can penetrate through the multilayer structure of the device to react with transport layers and perovskite crystals.<sup>8</sup> These reactions, leading to Lead Iodide formation, cause the degradation of the perovskite layer and the loss of the photoelectrochemical properties of PSC. Additionally, both perovskite and spiro-OMeTAD (i.e. the most widely employed Hole Transporting Material (HTM) in n-i-p PSCs) partially suffer for extreme and prolonged UV irradiation.<sup>9</sup> Domanski *et al.*<sup>10</sup> and Ajay Kumar Jena *et al.*<sup>11</sup> demonstrated that perovskite device performances deteriorate mainly because of the modification of the interface between the perovskite and spiro-OMeTAD at high temperature<sup>12</sup> and of the gold migration through the hole-transporting layer (HTL) exposing PSCs to a temperature of 70 °C.<sup>13,14</sup> In addition, the spiro-OMeTAD layer undergoes a severe morphological deformation showing large voids in it, which also reduces the cell performance.<sup>15</sup> It is worth mentioning that, if protected in a black box with an inert gas-saturated atmosphere, PSCs show a prolonged shelf-life stability.<sup>16</sup> Yet, to extend their sphere of application from laboratory scale to the industrial one, encapsulation of device is mandatory.

Degradation rates have been shown to fall exponentially when effective encapsulation/permeation barriers can be developed and applied to perovskite solar cells.<sup>17</sup> A good encapsulant/permeation barrier should provide: (i) transparency over the entire solar spectrum in order to not limit the absorption of the device, in light of application in tandem and semi-transparent stacks;<sup>18</sup> (ii) wide thermal stability: device experimented temperature higher than 70 °C (*in operando*)<sup>19</sup> and lower than -20 °C (during night-time in deserts);<sup>20</sup> (iii) good barrier properties toward both moisture and oxygen that cause the degradation of perovskite (PSK) and

HTM layers;<sup>21</sup> (iv) chemical inertness toward both contact and HTM (if applied onto the back of the cell);<sup>22</sup> (v) resistance to UVA and UVB radiation (if applied on the front-side) that usually caused the degradation of the PSK layer after prolonged exposure.<sup>23</sup>

As widely known, glass is one of the best encapsulating material because, on one hand, it possesses extraordinary barrier properties toward both oxygen and moisture (Water Vapour and Oxygen Transmission Rate, WVTR and OTR, up to  $10^{-5}$  g m<sup>-2</sup> day<sup>-1</sup> and  $10^{-4}$  cm<sup>3</sup> m<sup>-2</sup> day<sup>-1</sup> atm<sup>-1</sup> respectively when coupled with the adhesive)<sup>17,21</sup> on the other it almost completely filters UV radiation.<sup>24</sup> Yet, most glass covers need sealant to completely encapsulate the device. This sealing process usually requires temperature higher than 80 °C and/or pressure application that could degrade the devices. Additionally, most of the adhesives are not chemically inert toward perovskite film.<sup>17</sup> Moreover, when applied in PSCs, glass-based encapsulation almost doubles the overall weight of the device, leading to a halving of the photoconversion/weight ratio.<sup>25</sup> This could heavily jeopardize a feasible and cost-effective implementation at the industry scale. In this context, a great amount of effort has been recently made to realize glass-free encapsulation.<sup>26</sup> For example, Dameron *et al.*<sup>27</sup> reported on the use of multilayer of various metal-oxide (*i.e.* Al<sub>2</sub>O<sub>3</sub> and SiO<sub>2</sub>) deposited by Atomic Layer Deposition (ALD) one on the top of the other. Such an approach allows to obtain very low WVTR and OTR ( $10^{-5}$  and  $10^{-3}$ , respectively), but the cost effectiveness of this deposition technique has still to be demonstrated. Recently, Choi and co-workers used ALD to deposit a 50 nm-thick layer of Al<sub>2</sub>O<sub>3</sub> with good barrier properties (WVTR =  $1.8 \cdot 10^{-2}$  g m<sup>-2</sup> day<sup>-1</sup>).<sup>28,29</sup> Compared to inorganic encapsulant materials and related deposition processes, organic counterparts (*i.e.* polymers and polymer-based composites) show some advantages such as tuneable properties, lower production and deposition cost and the application on flexible device.<sup>30</sup> Nevertheless, they usually have relatively lower barrier properties in most cases not below 1 g m<sup>-2</sup>

$^2 \text{ day}^{-1}$ , if referred to a single polymeric material.<sup>21</sup> Composite encapsulants, *i.e.* organic-inorganic mixed films,<sup>31</sup> could be also employed but their synthesis is usually more expensive.<sup>32</sup>

Therefore, the development of a low-cost, effective, light weight and easily scalable encapsulant is a crucial, still unsolved, point for the forthcoming commercialization of PSCs.<sup>33–36</sup> Scientists have mainly focused their attention on encapsulant materials with barrier properties reaching or exceeding  $10^{-5}$  and  $10^{-3}$  for WVTR and OTR, respectively. Yet, all materials do not comply with these very strict requirements have been simply (and maybe too quickly) ruled out.<sup>21</sup> It is worth mentioning that these values refer to preformed films to be sealed onto the device. However, for liquid encapsulant, directly casted on the device and then hardened, the effective barrier parameters can be substantially different from the self-standing film ones. It should be pointed out how the critical figure of merit is not the barrier property itself, but the critic amount of water/oxygen reaching the device. Indeed, in ambient atmosphere a WVTR of  $10^{-3} \text{ g m}^{-2} \text{ d}^{-1}$  may cause the death of device after 1000 days.<sup>37</sup>

Following the above mentioned considerations, it is clear that there is not any report of the use of thermosetting polyurethane-based (PU) material used as encapsulant for photovoltaic devices, being their WVTR value just acceptable (*i.e.*  $0.1\text{--}100 \text{ g m}^{-2} \text{ d}^{-1}$ ).<sup>38</sup> However, albeit modest values of WVTR and OTR, this class of materials (aliphatic thermosetting PUs) possess some ideal features such as high transmittance (above 90%), chemical inertness and good UV and thermal stability if properly modified. Additionally, PUs are cost-effective, do not require cost-demanding polymerization procedure, could be flexible and therefore very promising for flexible PSC and/or OPV and their mechanical and optical properties can be easily tuned by changing the precursors or by adding filler/additives.<sup>39</sup> Very interestingly polyurethanes have been already applied as effective additives in the perovskite precursor mixture leading to improved stability of the resulting

layer.<sup>40,41</sup> Polyurethanes are a peculiar class of polymers made by step-growth polyaddition (SGP) of isocyanates and alcohols to form urethane bond. The mechanism of SGP consists in consecutive addition steps starting from the mixture of monomers (di-isocyanates and bi- or multifunctional alcohols) leading to the formation of linear thermoplastic (TPU) or branched thermosetting (PU), polyurethanes of increasing molecular weight.<sup>42</sup> In some case, one of the precursors can be a multifunctional oligomer or polymer containing functional groups in its backbone. Last but not least, PUs can be easily recycled.<sup>43</sup>

Usually, thermoplastic polymers have been employed as co-encapsulant in conjunction with a glass slide or simply as edge-sealant. The most efficient polymeric encapsulants for PSC and their performances are resumed in table S1 and are compared with state-of-art encapsulant materials. According to the S1 table just few reports referred to thermosetting polymers as stand-alone encapsulant. Among them, the best results have been obtained with UV-cured fluoro-polymers.<sup>44</sup> In all the other examples with thermoplastic polymers the photovoltaic performances of the device are not even monitored. By using thermosetting PUs just as back encapsulant is likely arduous to reach the stability proposed by Bella et al. with F-polymers;<sup>44</sup> notwithstanding PUs possess key advantages of being cheaper, more easily recyclable than F-polymers and more scalable.<sup>43,45,46</sup> Indeed, thermosetting PUs have been actively used as protective polymers in electronic application (*e.g.* LEDs).<sup>47</sup> Moreover, they could be drop-casted or deposited by spin- or blade-coating onto the device in an open environment and they do not required any external source to induce the polymerization, as it simply occurs at room temperature. Indeed, polymerization process could be speeded up by the employment of relatively high temperature and energetic radiation that could, in turns, induce the degradation of the perovskite film. Very recently, Fu *et al.* already demonstrated the superior barrier properties of a thermoplastic polyurethane, TPU, (compared to

Polyolefin Elastomer (POE) and ethylene vinyl acetate polymer (EVA)) as co-encapsulant materials for PSC.<sup>48</sup> Indeed, they employed TPU as sealing agent (*i.e.* at the edge) in conjunction with a glass frit, that acts as the main encapsulant. It is worth mentioning that TPUs and PUs substantially differ for the polymerization geometry, being the former linear and the latter branched: therefore, TPUs are mainly employed as thermoplastic sealant whereas thermosetting PUs should be polymerized directly in contact with the surface that has to be protected/encapsulated. However, the addition reaction occurs without the formation of any by-product molecules (*i.e.* water, alcohols, CO<sub>2</sub>): this is a key advantage of this class of polymers opening the way to the application by drop-cast onto a photoelectrochemical device followed by *in-situ* polymerization.

In this paper, we demonstrate, for the first time, how thermosetting resins based on polyurethanes (hereafter simply named polyurethanes) could be effectively employed as simple back encapsulant providing an effective moisture and oxygen barrier, with the glass substrate acting as front encapsulant. We specifically report on the application of PU as encapsulant in planar direct PSCs. This type of architecture is particularly advantageous thanks to the low-temperature solution fabrication (<180 °C), which allow its application in flexible devices too.<sup>49</sup>

The encapsulation is performed depositing two precursors onto the back of the device (*i.e.* in contact with both HTM and Au) to assure a close interaction between the external layer of the device and the PU. We mainly focused our attention on moisture and oxygen protection more than on photochemical stability. Nevertheless, encapsulated device showed also improved stability under continuous irradiation. Very interestingly, PU-encapsulated devices retain more than 94% of its initial efficiency after 2500 hours (*i.e.* > 100 days) when stored in laboratory environment. One should notice that the results reported throughout the present manuscript are at the initial stage



but, at the same time, they allow to classify thermosetting PUs as “worth-to-investigate” materials, contrarily to what usually stated by the perovskite community.

## 2. Results and Discussion

### 2.1. Selection of the PU

Aiming at choosing the most suitable polyurethane-based thermosetting polymer, we screened six different bi-component resins obtained combining three different diisocyanate precursor (IC) mixtures mainly based on two aliphatic molecules (*i.e.* hexamethylene-diisocyanate, HDI, and isophorone diisocyanate, IPDI) and two polyol (PO) formulations (**Figure 1**). The POs and ICs formulations differ in the pre-polymerization degree and in the HDI/IPDI ratio, respectively, leading to polyurethane-based resins with tuneable mechanical properties (see experimental section). The formation of the PU is a complex process. A relatively fast first step consists in a polyaddition reaction involving the majority of isocyanate moieties of IC and the hydroxyl groups of (partially pre-polymerized) PO. This leads to the formation of a great amount of novel urethane bonds organized in long polymeric chains just poorly interconnected. The second step, quite a slower kinetic, consists in a limited number of addition reactions involving the already formed polymeric chains to obtain a three-dimensional and highly crosslinked polymer.<sup>50</sup>

The main properties of the six PUs obtained with the various precursors are summarized in **Table 1**. The use of PO1 leads to less flexible (*i.e.* higher Shore D) polymers compared to the one obtained with PO2. It is worth mention that the flexibility of the polymers could be further tuned by the thoughtful choice of the diisocyanate. Therefore, PO2 was selected as polyol precursors and polyurethanes obtained after the polymerization with the three ICs (namely IC1, IC2 and IC3) were deeply investigated. Thermal stability of the polymers is just slightly influenced by the choice

of the IC precursor: the decomposition temperature,  $T_d$ , varies from 330.3 (PU21) to 327.7 (PU22) to 321.8 (PU23) according to the different HDI/IPDI ratio (see **Figure S1-S3**). Thermal degradation of all the polymers is completed at 400 °C. On the other hand, Differential Scanning Calorimetry (DSC) evidenced meaningful differences in the glass transition temperature ( $T_g$ ) of different PUs: indeed, PU23 showed the lowest  $T_g$  (*i.e.* 8.5 °C) whereas an increase is recorded for PU22 (*i.e.* 13.3 °C) and PU21 (*i.e.* 41.2 °C) as reported in **Figure S4-S6**. Straightforwardly, PU21 is discarded having a  $T_g$  higher than room temperature leading to more complicated and less controllable deposition process. We also investigate the PU surface affinity for water. Albeit PUs are usually considered hydrophilic polymers, the hydrophilicity/hydrophobicity of thermosetting PU strongly depends on both the reticulation degree of the polymers itself (*i.e.* the number of unreacted alcoholic moieties) and the nature of the R and R' groups in both the isocyanate and the polyol precursors (straightforwardly, the ratio between polar urethane residues and apolar groups).<sup>51</sup> Therefore, the simple definition of thermosetting PU as hydrophilic material could be highly misleading. As a matter of fact, polyurethanes are commonly used as sealants and water proofers in various industrial applications.<sup>46</sup> Moreover, the hydrophilicity/hydrophobicity is a property of the “surface” of the materials and it does not heavily impact its barrier properties. As a matter of fact, we measured the contact-angle (CA) of the selected film and value higher than 100° has been found (**Table 1**). As thoroughly reported in literature, a  $CA < 90^\circ$  indicates a “mostly hydrophobic” materials. More interestingly, once deposited onto the film surface, the water drop is highly stable, and it does not show any tendency to flatten or to permeate the PU layer.

It is worth mentioning that the values reported in **Table 1**, are measured for self-standing films, whereas the final application consists in a direct drop-cast of the precursor mixture onto the device followed by an *in-situ* polymerization. Therefore, some (slight) variations could be expected.

Arising from the characterization summarized in **Table 1**, we identified PU23 to be the most promising polymer to be employed as encapsulant in PSCs due to its lower  $T_g$ , higher flexibility and shorter first polymerization time ( $t_{fp}$ ) that can encourage an industrial and large-scale application. The  $t_{fp}$  is, in fact, the amount of time required for a roughly complete polymerization of the precursor mixture allowing to handle the sample and to easily delaminate it from the polymerization support.

## 2.2. Characterization of the self-standing PU films

Before employing the selected polyurethane-based resin (*i.e.* PU23) as effective barrier in Perovskite Solar Cells, we thoroughly investigated its optical and morphological features as well as its long-term stability under both thermal and UV-light stress. All the stress-tests were performed after the complete polymerization of the PU. The individuation of the actual time required for the complete polymerization is a crucial parameter to understand the ageing curves of encapsulated PSCs (*vide infra*). Concerning PU23, a first polymerization step (making the film wieldy) occurs in roughly two days whereas the polymerization process is completed after one week as proved by the Differential Scanning Calorimetry (DSC) analyses (**Figure S6**) in which there is not any trace of post-curing phenomena.

We investigated the thermal stability of PU23 layer by treating it at relatively high or very low temperature (*i.e.* in a conventional oven at 100 °C for different times or in a liquid N<sub>2</sub> bath, respectively). We mainly focused our attention on the possible modification of (i) the optical response of the films (*i.e.* transmittance of films in the UV-Vis region); (ii) the chemical degradation of the polyurethane layer. The latter phenomenon could be quite easily monitored by means of ATR spectra in which the presence of NH bending signal of urethane group (located at

1460  $\text{cm}^{-1}$ ) and the absence of the OH signal of the polyol precursors (located at around 3650  $\text{cm}^{-1}$ ) are a clear evidence of the retention of the polymeric matrix. As it is possible to see in **Figure 2a**, the thermal stress, even prolonged up to a week, did not cause any modification in the structure of PU23. The peaks located at 3350  $\text{cm}^{-1}$  and between 2850 and 3000  $\text{cm}^{-1}$  are associated to the stretching of NH and CH bond, respectively. Other meaningful peaks are the stretching modes of different moieties, *e.g.* CO (1700  $\text{cm}^{-1}$ ), NC (1460  $\text{cm}^{-1}$ ), COOR (1240  $\text{cm}^{-1}$ ) and COR due to R' chain (1095  $\text{cm}^{-1}$ ). The presence of NH is also confirmed by the band associated to the its bending, at 1530  $\text{cm}^{-1}$ . The three sharp bands located between 1300 and 1400  $\text{cm}^{-1}$  are due to the presence of organic molecules (dissolved in the polyol formulation) behaving as UV-stabilizers. Quite remarkably, the absence of the characteristic band of isocyanate group (at 2270  $\text{cm}^{-1}$ ) in the spectra of pristine PU23 is a key prove to verify the complete polymerization of the film.

The degradation process of polyurethane matrix starts at about 200 °C leading to partial volatilization of the polymer, due to pyrolysis and the formation of a charred residue thermally stable at 400 °C, as proved by Thermo-Gravimetric Analyses (TGA, **Figure S3**). To verify if a prolonged thermal treatment (below 200 °C) could somehow induce an irreversible degradation of the polymeric matrix, causing a substantial decrement in the barrier features of the PU, we recorded the UV-Vis spectra of a thermally aged sample: any possible change in the transmittance profile of PU23 could be ascribable both to a damaging of the film or to a degradation of the UV-stabilizers. As it is possible to see in **Figure 2b**, the optical profile of PU23 remained constant even after one week (*i.e.* 288 hours) of ageing at 100 °C.

The  $T_g$  of PU23 was evaluated by means of DSC and was found to be close to 9 °C. This temperature defines the cooling limit of 10 °C at which the PU film undergoes a hardening process and experiments a decrease in its flexibility. This could cause some irreversible modification in

the chemical structure of the polyurethane and/or some cracks throughout the film thickness. The occurrence of both cracks and matrix modification should be largely avoided to preserve the barrier features of the encapsulant. To verify the behaviour of PU23 at very low temperature, we stored self-standing films of polyurethanes in a fridge (4 °C), freezer (-20 °C) and ultralow-temperature freezer (-80 °C) for 3 days. Interestingly, meaningful modification in both optical and morphological features could not be noted. Therefore, to further stress the PU23 film, we dipped it in a dewar (containing liquid nitrogen, -196 °C). The film integrity was checked by means of both optical microscope and UV-Vis spectroscopy; if the film is damaged by temperature treatment, macrocracks would be easily highlighted by microscope, whereas microcracks and/or modification in the polymeric matrix (e.g. hyper-crosslinking of the polyurethane) would lead to a decrease in the film transmittance. After being removed from the dewar, the film was heated-up at room temperature and then analysed. Both optical microscope and UV-Vis analyses (**Figure 2c**) did not show any substantial changes in the polymeric matrix. This demonstrates that, even if some changes occur during the low-temperature treatment, they are completely reversible.

Furthermore, we also investigated the possible self-standing film degradation caused by the continuous UV-irradiation. It is worth mentioning that, throughout this paper, we mainly focus our attention on the barrier properties (toward both moisture and oxygen, *vide infra*) of PU23. However, good resistance under UV-stress is an added benefit to assure the long-term stability of our encapsulant. We continuously stressed the self-standing film of the polymer under UV light for up to 48 hours. This experimental set-up is highly stressing because, during the test, the internal temperature of the chamber reaches 130 °C. Very interestingly, the sample did not show any clear modification in its optical features (**Figure 2d**). The value of the optical cut-off, i.e. the wavelength at which the optical radiation is completely filtered, remains constant. As a matter of fact, any

change in the latter may be considered a red flag of the degradation of UV-protectors embedded in the polyurethane matrix.

Before using PU as encapsulant material on the solar cells, we evaluated the barrier properties of our films toward both the oxygen and the water vapour. As clearly stated in the introduction, encapsulants should comply with very strict parameters. The experiments made on our samples yields a WVTR and an OTR of  $61.6 \text{ g m}^{-2} \text{ day}^{-1}$  and  $256.6 \text{ cm}^3 \text{ m}^{-2} \text{ day}^{-1} \text{ atm}^{-1}$ , respectively (**Figure 2e-f**), measured with a MultiPerm instrument (see experimental section) showing inadequate values if compared to literature reports. Yet, our encapsulation approach is substantially different from the ones reported in the literature. In fact, the most common strategies employ barriers which consist of self-standing films applied onto the device and sealed with specific glues (usually epoxydic ones) which have been shown to be very sensitive to handling and application procedures..<sup>17</sup> Here instead we directly drop-cast the precursor mixture on the device and let it harden. It should be pointed out that the barrier properties of the *in-situ* polymerized film could substantially differ from the self-standing films. Therefore, we attempted a more realistic evaluation, but an ITO-sustained film could not be analysed with the same approach (see experimental section), being the glass a better barrier. We also attempted a different method to estimate the WVTR, namely the so-called Calcium test in which the WVTR of a barrier is related to the (optical or electrical) degradation rate of a cutlet of Calcium.<sup>52</sup> Unfortunately, this mixture quickly reacts with calcium making impossible to determine any value from these tests.

### 2.3. Application of PU films onto multilayer device

Once the good stability of PU23 under both thermal stress and UV irradiation was verified and knowing the intrinsic barrier properties (WVTR and OTR) of a 350- $\mu\text{m}$  thick self-standing film,

we decided to test our thermosetting resin as encapsulant in perovskite solar cells. Our approach consists in the deposition of the liquid mixture of the two precursors of PU23 directly onto the back of a n-i-p PSC, *i.e.* over both the Au contact and the HTM layer (in the space between the evaporated electrodes), and its polymerization *in situ* (see experimental section and **Figure S7**). It should be pointed out that thermosetting PUs could be also easily spin or blade-coated onto different substrates, in order to more finely tuning the thickness of the encapsulant layer. Nevertheless, to employ the latter approaches a further engineering of the small-area device is required, *i.e.* the contact should be protected. Very interestingly, the HTM is substantially inert to the IC/PO mixture. This allows us to not protect the latter during the drop-casting of the encapsulant. The thickness of the completely polymerized PU23 layer was estimated to be  $345 \pm 23 \text{ }\mu\text{m}$ .

Before starting the characterization of the complete devices, we investigated the effect of the direct polymerization of PU23 onto uncomplete stack (*i.e.* TCO/SnO<sub>2</sub>/PSK/HTM). Notwithstanding the modest barrier properties measured, the effect of the addition of PU as encapsulant material onto Perovskite (PSK) is dramatically evident: after two days the unencapsulated stacks suffer from a severe yellowing of the perovskite layer ascribable to the degradation of the PSK crystals into lead iodide (PbI<sub>2</sub>). On the other hand, the encapsulated stack does not present any evidence of degradation even after 100 days (**Figure S8**). Encapsulated and unencapsulated stacks were characterized by means of X-Ray diffraction (XRD, Mo K<sub>α</sub> or Cu K<sub>α</sub> source) to investigate the moisture induced modification in the perovskite layer. The test was performed on a PSK layer deposited directly on glass/TCO substrates. Albeit the choice of two different X-ray source could be somehow confusing to the reader, we were forced to do so. As a matter of fact, we employed Mo K<sub>α</sub> source to compare encapsulated and not encapsulated devices

in order to minimize the shielding effect of the polyurethane film. Indeed, the latter is relatively thick (0.3 mm) if compared to the PSK film and, even if it is composed only by light nuclei (*i.e.* H, C, O and N), it partially masks the contribution arising from the active layer. Therefore, when we used Cu  $K_{\alpha}$  to analyse the encapsulated film, both the (100) of the PSK and the (003) of the  $PbI_2$  are completely masked by the broad peak ascribable to the (amorphous) polyurethane. On the other hand, we need Cu  $K_{\alpha}$  when the aged films are investigated in order to enhance the surface sensitivity of the technique.

Before starting the measurements, the samples were stored under vacuum to minimize any interaction with air during the polymerization of the PU23. After two days, the samples were removed from vacuum and analysed. The diffractograms (Mo  $K_{\alpha}$ ) of both stacks are reported in **Figure 3a**. Some characteristic peaks ascribable to the crystallographic planes of perovskite (ICDD card #00-003-1114) could be evidenced: (100), (110), (111), (200), (210), (211), (220), (221) and (300), (222), (321) at  $2\theta = 6.38^\circ, 8.99^\circ, 11.05^\circ, 12.80^\circ, 14.32^\circ, 15.74^\circ, 18.23^\circ, 19.30^\circ, 22.36^\circ$  and  $24.25^\circ$ , respectively. Very remarkably, even though the unencapsulated sample was stored in vacuum during the polymerization of polyurethane matrix, it shows a more marked degradation compared the encapsulated stack as proved by the higher relative ratio between peak centred at  $5.76^\circ$  and  $6.38^\circ$  (Mo  $K_{\alpha}$ ) ascribable to (003) plane of  $PbI_2$  and the tetragonal phase of perovskite (plane (100)), respectively. It is worth mentioning that Mo  $K_{\alpha}$  allows to investigate a deeper section of the samples, being a more energetic radiation compared to classical Cu  $K_{\alpha}$  (0.717 Å and 1.540 Å, respectively). As a result of that, some peaks arising from TCO (planes (110), (101) at  $11.93^\circ$  and  $17.00^\circ$ , respectively) and  $TiO_2$  ((101) plane at  $15.19^\circ$ ) crystalline layers could be detected (green squares and light blue circles, respectively); the amorphous broadened peak between  $2\theta = 8^\circ$ - $16^\circ$  is due to the glass substrate. The latter is quite evident in the diffractogram



of unencapsulated sample whereas it is partially covered by the amorphous peak of polyurethane-based resin in the encapsulated sample one.

The presence of the peak at  $5.76^\circ$  in both the unaged samples is due to a not complete conversion of  $\text{PbI}_2$  into Perovskite crystal. It should be pointed out that the presence of  $\text{PbI}_2$  peak in the pristine film does not necessarily point towards a degraded photoactive layer, being, in small amounts, also beneficial for the PSC efficiency.<sup>53,54</sup> Yet, the unprotected device shows a higher intensity of the latter peak if compared to peak at  $6.38^\circ$  due to a quite fast degradation reaction occurring at the PSK/air interface. A  $\text{PbI}_2$ /PSK ratio of 0.32 and 0.65 is found for PU-encapsulated and not stacks, respectively. This ratio remains almost constant for encapsulated sample (**Figure S9**), whereas it dramatically increase in the exposed film (**Figure 3b**). To focalize the analysis on the modification of  $\text{PbI}_2$ /PSK ratio, we employed a less energetic radiation (*i.e.* Cu  $K_\alpha$ ) allowing to avoid the scattering of the glass substrate and to magnify the contributions of the top layers (*i.e.* lead iodide and/or Perovskite).

In this context, we specifically investigated the modification of the relative intensity of the first crystallographic peak of both lead iodide and perovskite; the intensity of both peaks referred to TCO (110) peak ( $26.48^\circ$ , green squares in **Figure 3b**). The latter was employed a normalization reference being nominally identical in all the samples. The analyses was limited at  $2\theta = 30^\circ$  angle (Cu  $K_\alpha$ ). According to Bragg's law, the change in the angles at which each reflection could be detected is due to the different source employed for this second set of measurements. As evidenced from **Figure 3b**, unencapsulated samples present a diffractogram that is sensibly influenced by the moisture exposure time. Indeed, the intensity of some typical peaks of the tetragonal phase of perovskite layer (*i.e.* (100) at  $14.03^\circ$  and (200) at  $28.38^\circ$ , brown triangles) gradually decrease whereas the (003) peak due to  $\text{PbI}_2$  (at  $2\theta = 12.68^\circ$ , red diamonds) become more and more

meaningful. Very interestingly, the intensity of PSK's (110) and (111) peaks also increase following on from the ageing of the samples. This means that the hydrolyzation of the perovskite film leads to a preferential growth of the (100) and (111) planes to the detriment of (100) and (200) ones. Furthermore, some additional signal ( $11.57^\circ$  and  $25.53^\circ$ ) could be evidenced following on from the ageing process. The attribution of the latter peaks is still being debated in literature, but they likely are due to some hydrated perovskite phases.<sup>55</sup> Other two small peaks, located at  $2\theta = 7.9^\circ$  and  $2\theta = 9.9^\circ$ , could be ascribable to 2D structure of the Perovskite<sup>56</sup> and they seems unsensitive to the ageing (but their intensity is really low to make some quantitative analyses). Concerning the  $\text{PbI}_2/\text{PSK}$  ratio (calculated from their more intense peaks) it changes from 0.33 (fresh sample) to 0.65 (sample being stored for 48 hours under controlled atmosphere, red trace in **Figure 3a**) to 0.81, 1.07 and 1.52 after 1, 7 and 24 hours of storage (at  $25^\circ\text{C}$  and  $\text{RH} = 60\%$ ), respectively (black, orange and purple traces in **Figure 3b**). The continuous ageing of unencapsulated sample leads to the disappearing of PSK peaks after roughly one week whereas the diffractogram of the encapsulated device remains unchanged over the same ageing period (**Figure S9**). To further confirm the cause of the degradation of unencapsulated device we performed some optical microscope analyses after storing the sample under controlled atmosphere (i.e.  $25^\circ\text{C}$  and  $60\% \text{RH}$ ). As recently proved by Di Girolamo *et al.* for  $\text{CsPbBr}_3$ ,<sup>57</sup> the interaction of moisture within PSK crystals leads to an initial growth of the latter (during the first 48 hours of exposure, **Figure 3d**) and to a subsequent merging of the different crystallites (**Figure 3e**). This phenomenon becomes irreversible after roughly 100 hours in a  $60\% \text{RH}$  environment (**Figure 3f**) being characterized by the complete merging of the crystallites. The findings evidenced by optical analysis are also confirmed by XRD spectra of aged samples (**figure 3b**) in which the intensity of perovskite hydrated phase (peaks at  $2\theta = 11.57^\circ$  and  $25.53^\circ$ ) increase with the exposing period. It

is worth mentioning that the encapsulated device did not evidence any significant modification in neither its morphological nor crystallographic structure.

## 2.4. Performance of Pu-encapsulated devices

Once the surprising barrier properties and inertness (toward both PSK layer and HTM) of the PU film were evaluated, we finally tested their effect on the PV performance of perovskite solar cells. The precursor mixture of the encapsulant was drop-casted onto the device in contact with both HTM and Au (see **Figure S7**) and let polymerize for one day. **Figure 3c** shows the shelf life measurements of the electrical parameters of different devices over a time span of 1200 hours stored according to ISOS-D1 (*i.e.* room humidity and temperature). It should be pointed out that, in order to assure an effective comparison between devices, the ageing test was started when the polymerization of the barrier is completed (*i.e.* roughly one week). During that time the devices are stored in glovebox. Straightforwardly,  $t=0$  in **Figure 3c** corresponds to  $t = 7$  days. Starting average efficiency of our cells (ITO / SnO<sub>2</sub> / Perovskite / Spiro-OMeTAD / Au) is 16%, which the is in line with most of the articles in the literature for low-temperature planar nip solution processable PSCs.<sup>58–60</sup> The unencapsulated devices show a more pronounced decrement in photoconversion performances compared to encapsulated counterparts losing more than 10%, 20% and 30% of their initial value after 100, 700 (this is the T80 value of unencapsulated device) and 1150 hours, respectively. On the other hand, encapsulated devices do not reach T80 within the investigated timeframe. **Figure S10** shows the shelf life measurements of the electrical parameters of different devices over a time span of 2500 hours stored in ambient conditions (*i.e.* 28-65% RH and temperature ranging from 18 to 30 °C). In addition to this experiment, we performed another characterization on solar cells stored on the lab shield in order to evidence some eventual light-

induced degradation phenomena of the PU film. Indeed, considering that thin film perovskite solar devices have proven potential to power indoor devices for applications such as smart homes, internet of things etc.<sup>61</sup> that often do not need to last over 25 years but much less, stability improvement even in ambient conditions can be of significance. As expected, this ageing test is more stressing than ISOS-D1. The unencapsulated devices shows a decrement in photoconversion performances (**Figure S10**) losing more than 20%, 50% and 80% of their initial value after 37 (this is the T80 value of unencapsulated device), 125 and 300 hours, respectively. On the contrary, encapsulated devices retains more than 93% (best 96%) of their initial value over 2500 hours. Concerning encapsulated devices, T80 was not reached within the investigated timespan; yet, the so-called back extrapolated T80 could give an effective estimation of this parameter:<sup>62</sup> the latter is 6850 hours (*i.e.* 285 days) being 185-fold the equivalent value of unencapsulated devices.

Unencapsulated devices initially suffer a decrease in photocurrent (**Figure S11a**) followed by one in both FF and  $V_{OC}$  (**Figure S11b-c**) resulting in a drop of over 80% of their initial power conversion efficiency in just 300 hours (**Figure S11d**). It is worth mentioning that the ageing profile of PU23-encapsulated devices is not so straightforward: in the first days after the encapsulation, the photoconversion efficiency of the devices decreases faster than reference ones (showing a drop of 35%, **Figure 4a**). Then, after 2 days there is a partial recovery of the photoactivity and the electrical figures of merits became stable after one week retaining their performances (93% of initial PCE) for 2500 hours.

The initial drop of all the photovoltaic parameters is consistent with the timeframe of the *in situ* polymerization process.<sup>50</sup>  $J_{SC}$  (**Figure 4c**) seems to be the most influenced among photovoltaic parameters by the polymerization process; compared to fresh device, it experiments a severe decrease (-30%) probably due to the interplay between the liquid precursor mixture and the HTM

that may reduce the charge transport properties of the latter. This also impacts on the  $V_{OC}$  (**Figure 4b**) that is 5% lower than the fresh devices. Nevertheless, once the latter process ended (or at least substantially slowed down)  $J_{SC}$ ,  $V_{OC}$  and  $\eta$  rise again approaching the values of pristine device (**Figure 4b-c**). Polyurethane polymerization is a complex thermoset process. Its kinetic is affected by factors like the composition of the reaction mass, type of catalyst, and possible side reactions.<sup>63</sup> Remarkably, we found a strong correlation between the polymerization kinetic of polyurethane-based film (**Figure 4d** and **S12a**) and the recovery trend of photovoltaic parameters. After the initial drop, as far as the rate of the polymerization process slows down (**Figure S12b**), the photoconversion efficiency of encapsulated device increases continuously. Once the polymer is completely crosslinked (**Figure 4d**), the photovoltaic parameters reaches a constant value too. For further details on this correlation see SI (**Figure S12** and related discussion).

This unprecedented behaviour could be ascribed to an interaction between the encapsulant materials and the HTM. As a matter of fact, when deposited onto the device, the precursor mixture is still in its liquid form. It is reasonable to believe that the PU mixture cannot penetrate the gold electrode. However, it will get in contact with the uncovered portion of the HTM layer which is easier to permeate for the PU in its liquid form. Once permeated into the HTM it could diffuse throughout the layer allowing a strong adhesion of the material. Albeit further studies are obviously required to deeply understand the mechanism of device/encapsulant interaction, the HTM permeation hypothesis befits experimental results: as showed in **Figure 4e**: once mechanically delaminated from the device, the PU film appears yellow. The colour is likely due to the HTM (*i.e.* spiro-OMETAD) strongly interacting with the polymeric encapsulant. A strong interaction between gold and PU is also expected, as already reported in literature.<sup>64</sup> This is particularly appealing considering a forthcoming application of PU-based resins in large-area device in which

the majority of expose area is made by back contact. On the other hand, the PSK layer is still adherent to the TCO substrate. This proves that the encapsulation process does not directly influence the photoactive layer that is actually protected by the HTM (in the stack configuration) and both HTM and gold (in complete devices). Indeed, if PU mixture would penetrate the HTM and interact with the perovskite layer some morphological and phase modification of the latter could be fairly expected. Yet, as also proved by XRD analyses, **Figure 3a**, no changes could be evidenced following on from the encapsulation of the stack.

As it is possible to see from **Figure 4b**, after a stabilization period (first 250 hours from the encapsulation), the open circuit voltage of the encapsulated device is systematically higher than the value of the fresh device. In Perovskite Solar Cells, the theoretical  $V_{OC}$  value is limited by the energy gap of the photoactive material (*i.e.* the difference between Conduction and Valence Band of Perovskite film).<sup>65</sup> Yet, the real value could be reduced by both dark current and recombination reactions.<sup>66</sup> In our case, a modification in the Perovskite electronic structure of encapsulated device is mostly unlikely, being the polymeric matrix not able to penetrate PSK layer (**Figure 4e**). Therefore, the higher  $V_{OC}$  is tentatively ascribed to a decrease in losses due to the interaction between polyurethane-based matrix and HTM layer and/or gold electrode. An enhancement in the quality of the PSK/HTM interface cannot be excluded. We are aware that, in the literature, a higher  $V_{OC}$  compared to the fresh device is also ascribed to different factors: Fei *et al.*<sup>67</sup> proved that the air exposure (48 hours) of  $SnO_2$ -based PSCs could lead to an age-induced re-crystallization of the perovskite layer suppressing both trapping and recombination of charges ameliorating the transport properties of the active layer; Liu *et al.*<sup>68</sup> observed that a controlled exposure (24 hours) of spiro-OMeTAD to oxygen could lead to the formation of spiro-OMeTAD<sup>+</sup> and to longer-living hole carriers; finally, Lee *et al.*<sup>69</sup> postulate a bettering of the PSK/ETL interface with time due to the

self-passivating properties of  $\text{SnO}_2$  reaching a plateau value after 100 hours. Albeit these effects could not be completely ruled out, they are quite unlikely to be the reason behind the recovery of our devices, being the latter stored in dark for three days before encapsulating them. Therefore, if some of the former phenomenon occurred, it will result in the PCE value of pre-encapsulation device.

To further prove the beneficial effect of PU encapsulation, we performed light-soaking (LS) measurements on both encapsulated and non-encapsulated devices. During the aging test, cells are constantly operated at the MPP at room temperature under illumination; simultaneously, the photoelectrochemical performance is regularly monitored by extracting the photovoltaic parameters PCE,  $J_{\text{SC}}$ , FF and  $V_{\text{OC}}$ . It is worth mentioning that PU film is applied only onto the back of the device, whereas the illumination is provided from the front. Therefore, the radiation reaching the photoactive layer is exactly the same for both the devices being not filtered but for the front glass. Notwithstanding this, a better stability of encapsulated device is expected being the photoinduced degradation processes exalted by the permeation of both oxygen and water. Indeed, encapsulated devices evidenced a slightly higher photostability. It should be pointed out that, likely to ISOS-D1 measurements (**Figure 3c**), we did not expect the “drop and recover” PCE behaviour evidenced in **Figure S10** (*i.e.* aging in lab environment), being the LS measurements started after the polymerization of the PU is completed, roughly one week. During polymerization time, the cell were stored in controlled atmosphere in order to avoid any degradation: the PCE values of fresh sample were comparable to the one measured at  $t=0$  in LS measurements. **Figure 5** reports an average of electrical parameters of three devices normalized to the value obtained at  $t = 0$  min. The significant  $J_{\text{SC}}$  drop recorded for unencapsulated tested PSCs strongly reduces the device performance during the endurance test. The degradation of the light harvesting perovskite layer

explains the  $J_{SC}$  depletion with the aging. Actually, encapsulated PSCs allow to limit the PCE drop that is observed in the stability by showing a T80 (losing 20% of the initial PCE value) equal to 250 min of the stress test, whereas the PCE of the unencapsulated cells decayed by 60% over the same period (T80 equal to 52 hours). This indicates that the PU encapsulation can effectively reduce the aging effects in the PSCs and will improve the stability of PSCs in real operating conditions where light, temperature and moisture are combined.<sup>23</sup> Indeed, a possible explanation of such an evidence consists in the protecting action of the polyurethane layer and its extension throughout the HTM layer (**Figure 4e**): this partially avoids the moisture or oxygen from diffusing throughout the HTM layer and reaching the PSK layer. Therefore, the moisture/oxygen degradation processes are partially minimized. Moreover, PU23 may fill the voids commonly present in the HTM layer leading to a more hindered diffusion of photogenerated defects.

To further gauge the scientific and technological interest due to the implementation of PU23 as encapsulant material in Perovskite Solar Cells, we dipped our devices in a deionized water solution. The results were quite impressive (**Figure 6**): as expected, the unencapsulated device suddenly started to degrade becoming more and more yellow; after 120 seconds, the entire PSK layer was converted into  $PbI_2$  that tended to be quite rapidly (240 seconds) solubilized in water; after 5 minutes (approx.) the Au-based contacts were the only evidence of the original device. Remarkably, the PSK layer beneath the Au contact was degraded too. On the other hand, encapsulated device did not suffer any degradation process once immersed in water and appeared practically unchanged after more than 4 days. It is worth mentioning that a negligible degradation of the PSK layer of encapsulated device started after one day (last picture in **Figure 6**). Yet, this degradation occurred from the silver contacts (that were not fully masked to allow the testing of the device) and, straightforwardly, it could be easily avoided by an optimized engineering of the



device (*e.g.* with external contacts). Additionally, this issue would be easily avoided in module configuration. After six days of continuous dipping, the PSK layer of the encapsulated device was completely converted into  $\text{PbI}_2$  (*i.e.* total yellowing of the device). It is important to stress how the unprotected device reached the same status after only 60 seconds: this means that the degradation occurred roughly 9000 times faster. This evidence opens the door to possible application of PSC also in water (or moisture)-rich environment pointing out that a proper encapsulation of the device is a mandatory issue to be solved toward the commercialization of this technology.

Similar results could be in principle also obtained with conventional “encapsulation” methods (even though there are just few reports in literature).<sup>70</sup> Yet, as far as we are aware, *in-situ* polymerized PU-based resins are, up to date, the only technology allowing to obtain effective encapsulation properties being cost-effective and easily scalable avoiding complicated deposition method. Furthermore, being flexible, they could be effectively used also in flexible electronics (not limited to PSCs).

### 3. Conclusion

Throughout the present paper we report, for the first time, on the direct *in-situ* polymerization of polyurethane-based resins (without any additional encapsulant material) as effective, cost-effective and easy-scalable moisture and/or oxygen barrier in perovskite solar cells (PSCs). The most promising polyurethane-based resin were selected out of six different formulation; polyurethane-based self-standing films were deeply characterized to evidence any failure due to prolonged UV or thermal (both at 100° and -196° C) ageing. PU23 films showed low or insignificant degradation, *i.e.* they retain their initial morphological and optical features.

The encapsulated final devices showed a worth-to-notice stability (over 2500 hours) when stored in ambient condition retaining more than 90% of their initial efficiency. In the same experimental condition, the unencapsulated cell lost more than 20%, 50%, 80% and 99% of its initial value after 37, 125, 300, 2500 hours respectively. The improved stability was ascribed to the extremely good moisture and oxygen barrier properties assured from the PU film that prevented the degradation of the PSK film into PBI<sub>2</sub> as proved by XRD and optical microscopy.

Very interestingly, the implementation of PU film onto the back of the device slightly enhance the photostability of the PSCs too. The latter could be substantially improved by the employment of a protective layer onto the top of the device. Furthermore, when dipped in a deionized water solution, the encapsulated devices showed a stability 9000 times higher than the unprotected counterpart. This value could be sensibly enhanced by the further engineering of the electric contacts.

In-situ polymerized aliphatic polyurethane-based resins are a class of transparent barrier material allowing to obtain good retention of photoconversion efficiency over a prolonged ageing period being low-cost, easy to synthesize, tune and recycle, scalable, environmental-friendly and applicable to both rigid and flexible substrates..

## 4. Experimental Section

*Deposition of thermosetting PUs.* All the precursors are provided by SE Special Engines S.r.l.. Three different diisocyanate hardener (IC, namely IC1, IC2 and IC3) differing for the hexamethylene-diisocyanate (HDI)/isophorone diisocyanate (IPDI) ratio and two polyol formulations (PO, namely PO1 and PO2) with different pre-polymerization degree were formulated (SE Special Engines s.r.l.) and employed without any further modification. UV-

stabilizers are dissolved into the PO formulation to enhance the stability of the resulting polymer toward high energetic radiation. The IC and PO precursors were cross-combined (in a 1:1 w/w ratio) to obtain six different polyurethane-based polymers that were characterized as self-standing films. As soon as the polymerization process is completed, the PU layer was mechanically removed from the substrate surface. Polymerization time depends on the precursor nature and quantity (**table 1**). For the application as encapsulant onto PSCs, the IC/PO (1:1 w/w ratio) mixture was directly drop-casted onto the back side of the device, then treated under continuous vacuum for ten minutes to remove eventual air bubble produced during the mixing and deposition processes. Both film thickness and uniformity are expected to influence the encapsulation properties of barrier layer. To assure uniformity, we degassed the polyol-based precursor for 30 minutes under vacuum (in order to eliminate air bubble and/or water traces) and then we carefully drop-casting it onto the device; on the other hand, the encapsulant thickness could be controlled by the amount of precursors mixture that was drop-casted onto the devices.

*Characterization and ageing of PUs.* Self-standing films of the more promising PU (i.e. PU23) were aged in different condition (i.e. thermally stressed in an oven at 100 °C and under liquid nitrogen at -50 °C or optically stressed under continuous UV irradiation (Dymax EC-5000 Lamp). During ageing, their optical and morphological features were continuously monitored by means of both UV (UV-1700 PharmaSpec by Shimadzu) and IR (FTIR-8400 from Shimadzu) spectroscopy. Oxygen Transmission Rate (OTR) and Water Vapor Transmission Rate (WVTR) were measured on the self-standing polymeric films with a MultiPerm (ExtraSolution) instrument. The sample is inserted between two separated chambers and it acts as a membrane. Both the chambers are evacuated by using an inert gas (N<sub>2</sub>) leading to an Oxygen (or Water Vapor) concentration lower than 1 ppm. After that the desired gas is fluxed in the upper chamber and its concentration is

measured in the bottom one, until a stationary value is reached. The analyses are done keeping constant both temperature and relative humidity. The thermo-gravimetric analyses (TGA Q500 from TA Instrument) were performed on the polymeric film sealed on an aluminium plate heated from room temperature up to 800 °C with a heating rate of 20° C/minute. Before performing any DSC measurements (DSC Q200 from TA Instrument), the polymeric films were stored at 40 °C in vacuum overnight in order to remove residual water molecules adsorbed onto the surface, then, the samples were sealed in an aluminium pan and cooled from RT to -80° C. After being at that temperature for 5 minutes, they were heated up to 180° C with a heating ramp of 5 °C/minute and then cooled back at -85° C. This cycle was repeated twice in order to evidence any post-curing effect on the samples. To check the kinetic of the polymerization process we continuously recorded the IR spectrum (Spectrum Spotlight 300 FT-IR spectrometer from PerkinElmer) of the polymerizing sample: the mixture of precursors were deposited onto an aluminium foil and the IR spectra were recorder every hour till the process was ended.

*Preparation and storage of PSCs.* All the materials have been purchased at the highest degree of purity available. All solvent are purchased from Sigma Aldrich if not differently specified. Perovskite Solar device were fabricated as follow: Np-SnO<sub>2</sub> the 15% Tin (IV) oxide nanoparticles in H<sub>2</sub>O colloidal solution (Alfa Aesar) was spin coated in the air onto Glass/ITO substrates (Kintex 15 Ω/cm<sup>2</sup>) at 6000 rpm for 45 s. and then annealed in air at 100 °C for 1 hour. To make the perovskite precursor solution, 547.4 mg mL<sup>-1</sup> of PbI<sub>2</sub> (TCI), 87.1 mg mL<sup>-1</sup> of PbBr<sub>2</sub> (TCI), 21.6 mg mL<sup>-1</sup> of MABr (GreatCell Solar), 166 mg mL<sup>-1</sup> of FAI (GreatCell Solar) and 19.4 mg mL<sup>-1</sup> of CsI (Sigma Aldrich) were dissolved in mixed N,N-dimethyl sulfoxide (DMSO) and N,N-diethyl formamide (DMF) solvents (1:3.16 by volume) by stirring for 24h at room temperature. The as-prepared precursor solution was then spin coated in glove box (GB) onto the tin oxide film with

two steps spinning, first 1000 rpm for 10 s and then 5000 rpm for 30 s; 7 s before the end of the second spin coating step, 0.2 mL of chlorobenzene was dropped on the substrates. Afterwards, the perovskite layer (about 600 nm) was treated at 100°C for 50 min in GB. The hole transporting material (HTM), a solution of spiro-OMeTAD (from Borun) in chlorobenzene (CB) (73.5 mg/mL) with additives of lithium bis-(trifluoromethyl sulphonyl)imide (Sigma Aldrich) in acetonitrile (16.6  $\mu$ L, 520 mg/mL), of cobalt additive (7.2  $\mu$ L, FK209 from Sigma Aldrich, 0.25 M in acetonitrile) and 4-tert-butylpyridine (27  $\mu$ L, from Sigma Aldrich), was spin-coated at 2000 rpm for 20 s in air. Finally, the cells were completed by thermal evaporation of Au (80 nm) as the top electrode. Both PU-encapsulated and not encapsulated devices were stored onto a lab shelf (*i.e.* indoor illumination; temperature range: 18 °C-30 °C; RH ranging from 28 to 65%) without any additional protection and tested every 3-4 days. It is worth mentioning that an univocal testing protocol for PSCs have been only recently established.<sup>62</sup> Before of that, scientists usually refer to protocols commonly adopted for OPVs.<sup>29</sup>

*Characterization of (un)encapsulated devices.* X-ray Diffraction apparatus and optical microscope (Leica DM2500, max magnification 200x) were employed to evaluate the degradation of (un)encapsulated devices during shelf life. The powder X-Ray diffraction patterns (VTXRD) were collected with a X'Pert PRO MPD diffractometer from PANalytical working in Bragg-Brentano geometry equipped with a Cu K $\alpha$  source. Scattered photons were revealed by an X'celerator linear detector equipped with a Ni filter to attenuate K $\beta$ . WAXS experiments were carried out on a Bruker D8 Advance with DaVinci design diffractometer (angle dispersive). The diffractometer is equipped with a Mo K $\alpha$  X-Ray tube ( $\lambda = 0.7107$  Å). The scattered intensity was gathered with the Lynxeye XE Energy-Dispersive 1-D detector. For the electrical characterization of the devices we employed a custom-made system which allows to simultaneously measure all

the pixels of a device plate. They were carried out under a class A solar simulator (ABET Sun 2000) at  $1000 \text{ W m}^{-2}$  of flux density (scan rate  $60 \text{ mV/s}$  in reverse mode) with artificial solar spectrum AM 1.5 G whose lamp was calibrated with a pyranometer. The devices were masked with an aperture of  $0.1 \text{ cm}^2$  to define the active working area. All electrical contact have been covered with silver paste. The external quantum efficiency (EQE) spectra were collected as a function of wavelength using an optical power density-based measurement system (Arkeo from Cicci research s.r.l.) under the irradiation of  $300 \text{ W}$  Xenon lamp (Mod.70612, Newport). The light soaking stability test was accomplished under the illumination MPPT tracking system (Cicci research s.r.l.) composed by a white LED array ( $4200 \text{ K}$ ) tuneable up to  $2000 \text{ Wm}^{-2}$  of optical power density and a high-speed source meter unit.

FIGURES.

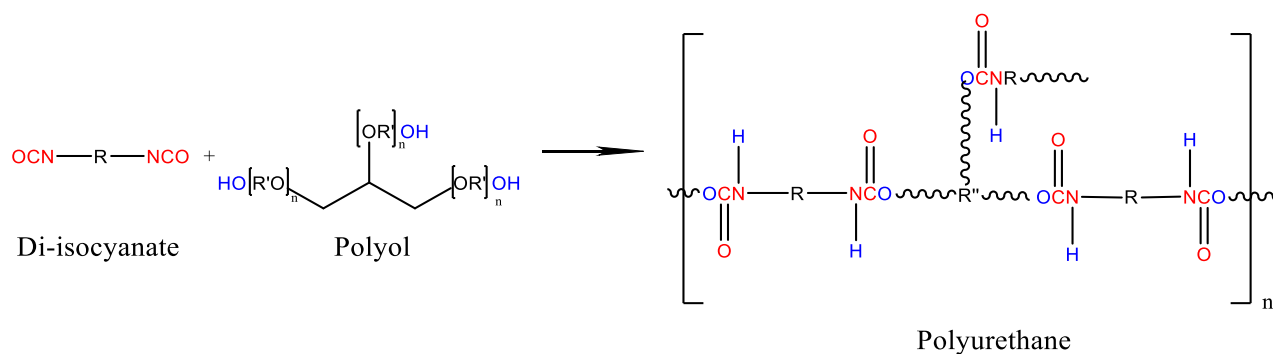


**Figure 1.** Schematic representation of the reaction to obtain polyurethanes resins in which R and R' have aliphatic structures and R'' is  $-\text{[R}'\text{O}]_n\text{-CH-CH[R}'\text{O}]_n\text{-CH[R}'\text{O}]_n-$ .

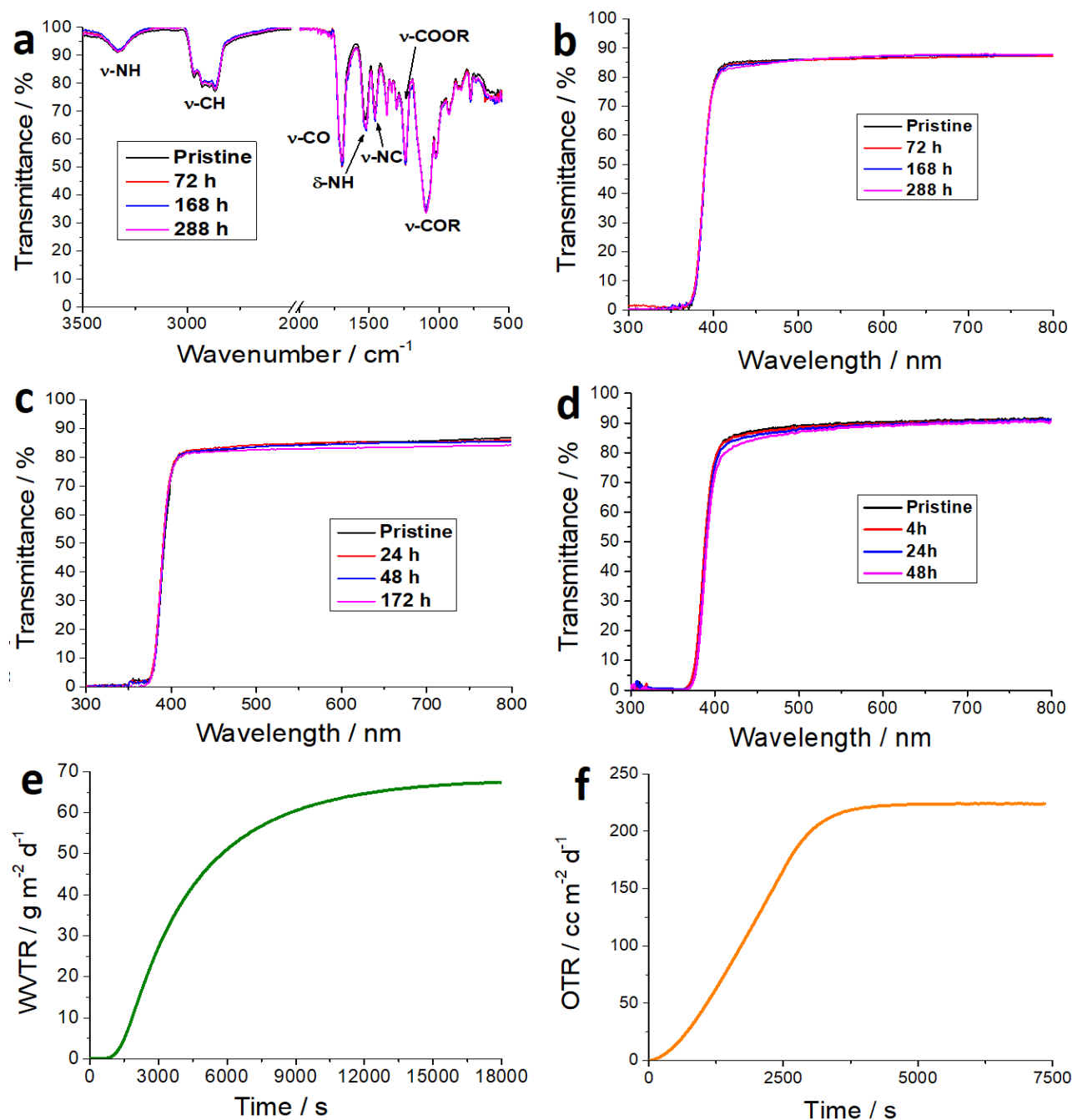


**Figure 2.** (a) ATR and (b) UV-Vis spectrum of thermally (up to 100 °C) stressed films of PU23 for different times; UV-Vis spectra of thermally (- 50 °C) (c) and UV (d) stressed self-standing films of PU23; Water Vapor Transmission Rate (WVTR, e) and Oxygen Transmission Rate (OTR, f) of the self-standing film of polyurethane based films (see experimental section for further details).

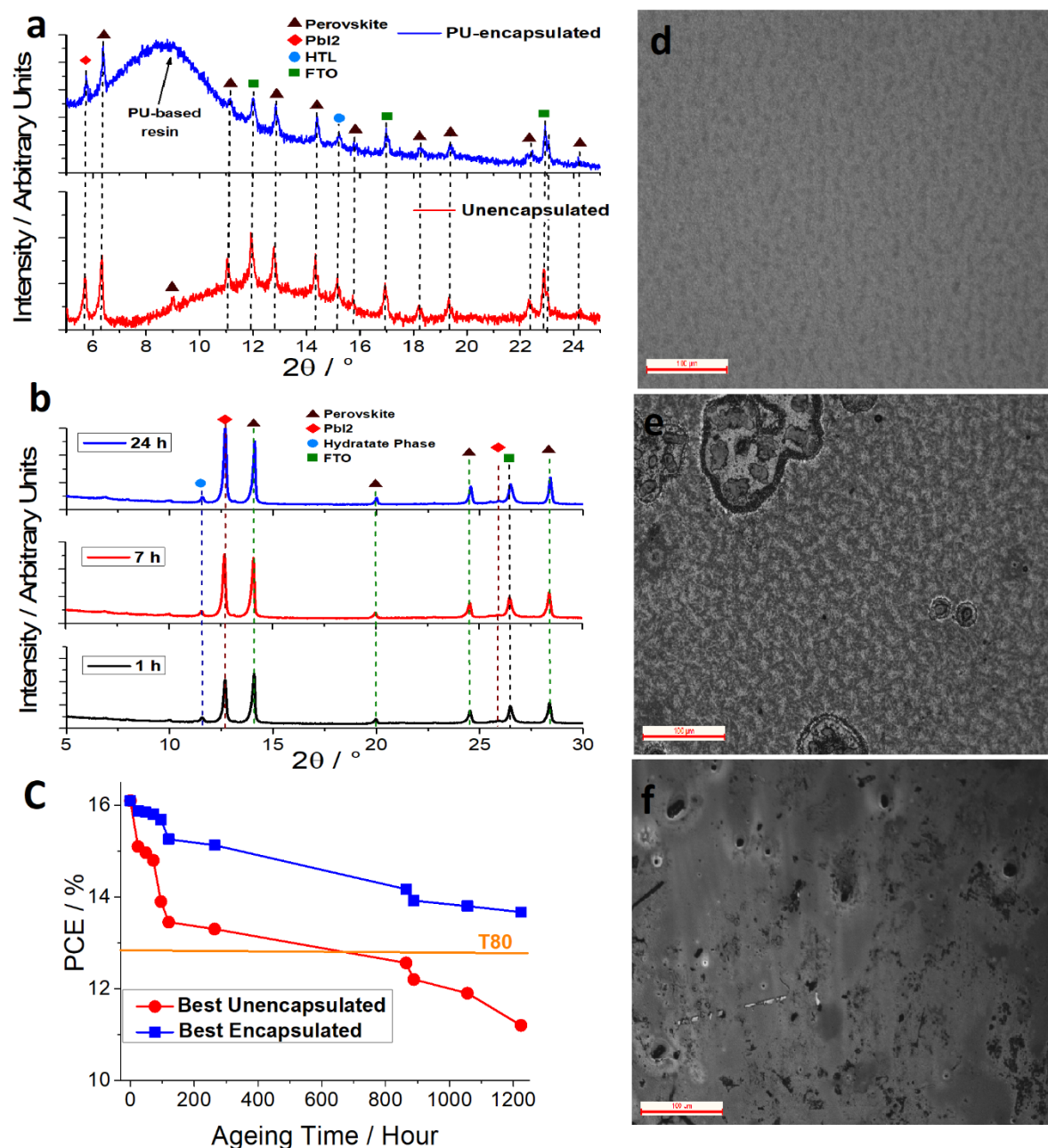


**Figure 3.** (a) XRD pattern of unencapsulated (red) and encapsulated (blue) device after two days of storage in controlled atmosphere; Mo K $\alpha$  was employed as X-ray source to allow the investigation of a deeper section; (b) diffractogram of unencapsulated samples after 1h (black trace), 7h (orange trace) and 24h (purple trace) of ageing time (stored at RH < 60% and T ranging from 20 to 30 °C); Cu K $\alpha$  was employed as X-ray source to perform a more surface-sensitive investigation; (c) comparison between power conversion efficiency (measured under 1 Sun AM1.5G) vs ageing time of unencapsulated (red dots) and PU23-encapsulated (blue squares) devices; ageing was performed complying with ISOS-D1 standard. Optical microscope images of unencapsulated PSK layer after 1 (d), 50 (e) and 24 (f) hours of ageing.



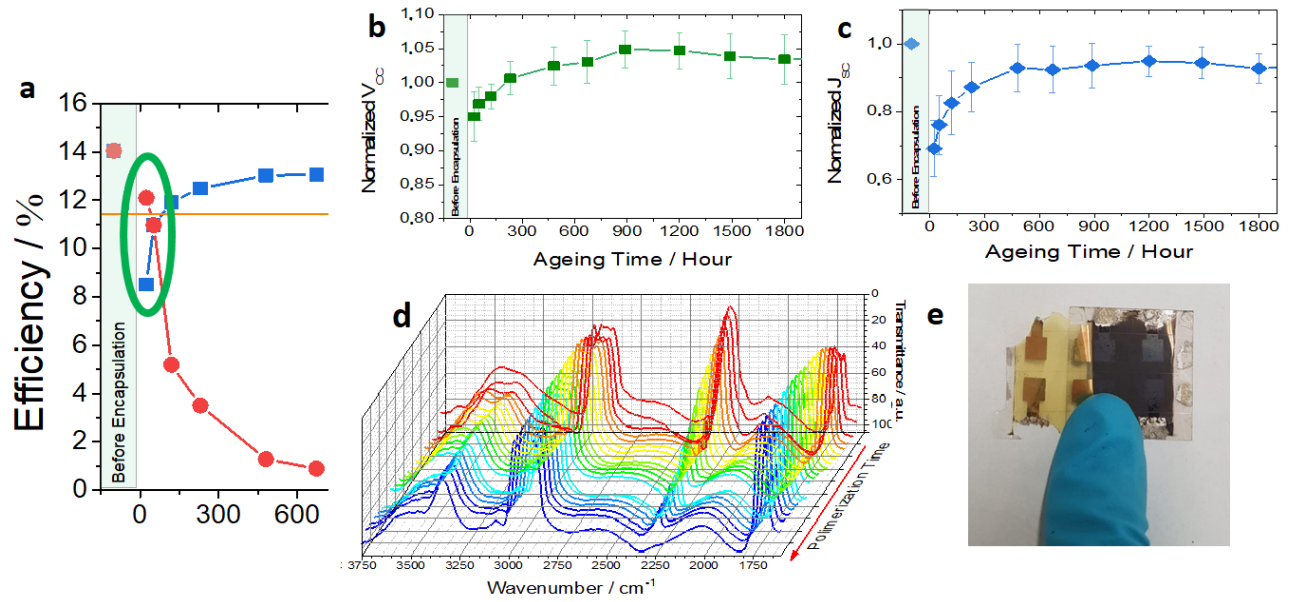


**Figure 4.** (a) Zoom of the first 600 hours of ageing for the most efficient encapsulated (blue squares) and unencapsulated devices (red dots); normalized photoelectrochemical parameters (*i.e.*  $V_{OC}$  (b);  $J_{SC}$  (c)) of encapsulated devices within the ageing period (measured under 1 Sun AM1.5G). (d) FTIR spectra of the polymerizing mixtures; (e) digital photograph of the delaminated PU-based encapsulant.

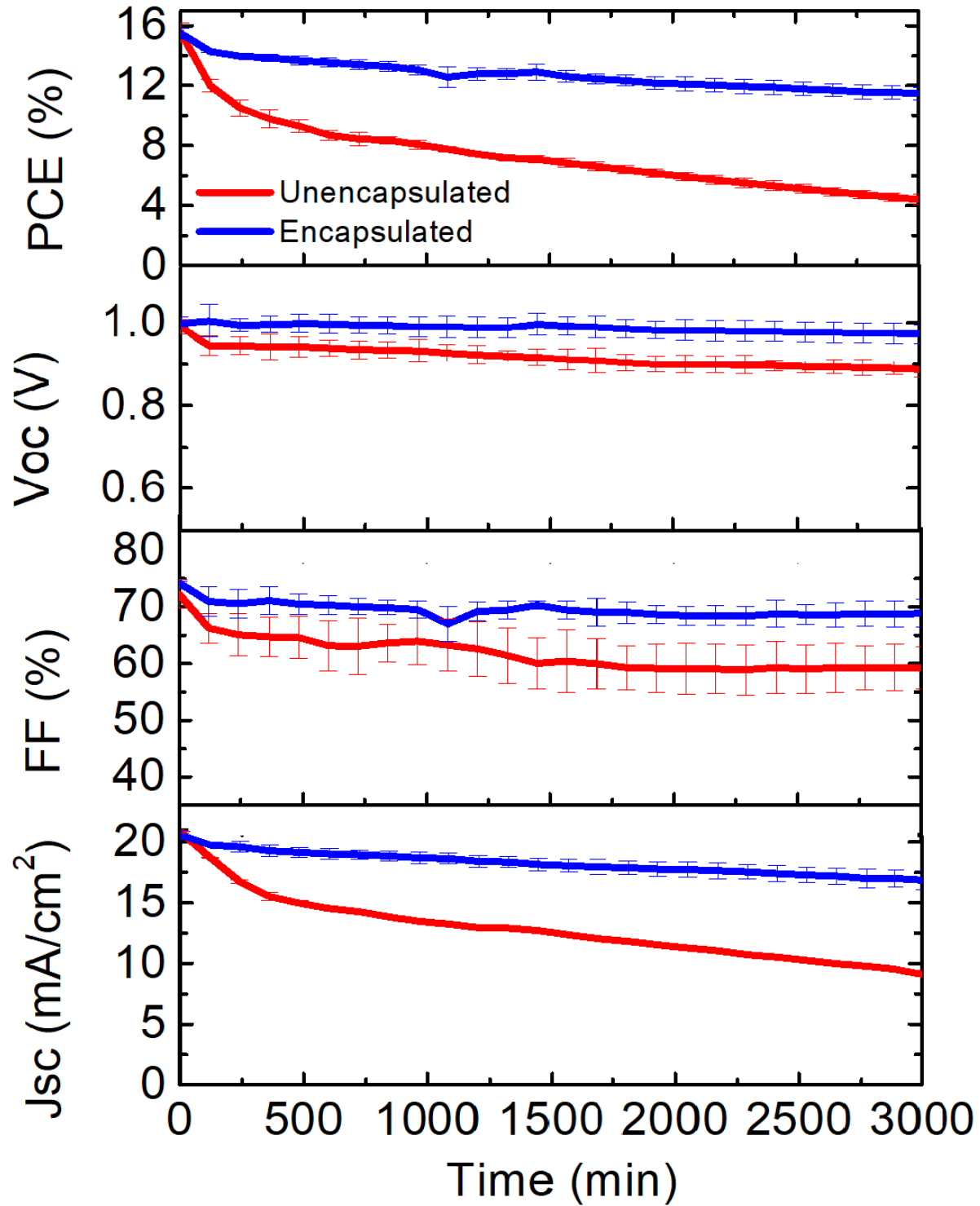


**Figure 5.** Normalized photovoltaic parameters ( $V_{oc}$ ,  $J_{sc}$ , Fill Factor and PCE first, second, third and fourth graph, respectively) extracted from light-soaking measurement of encapsulated (blue lines) and unencapsulated (red lines) devices. Value are averaged between five namely identical devices. The light soaking stability test was accomplished under the illumination MPPT tracking system composed by a white LED array (4200 K).

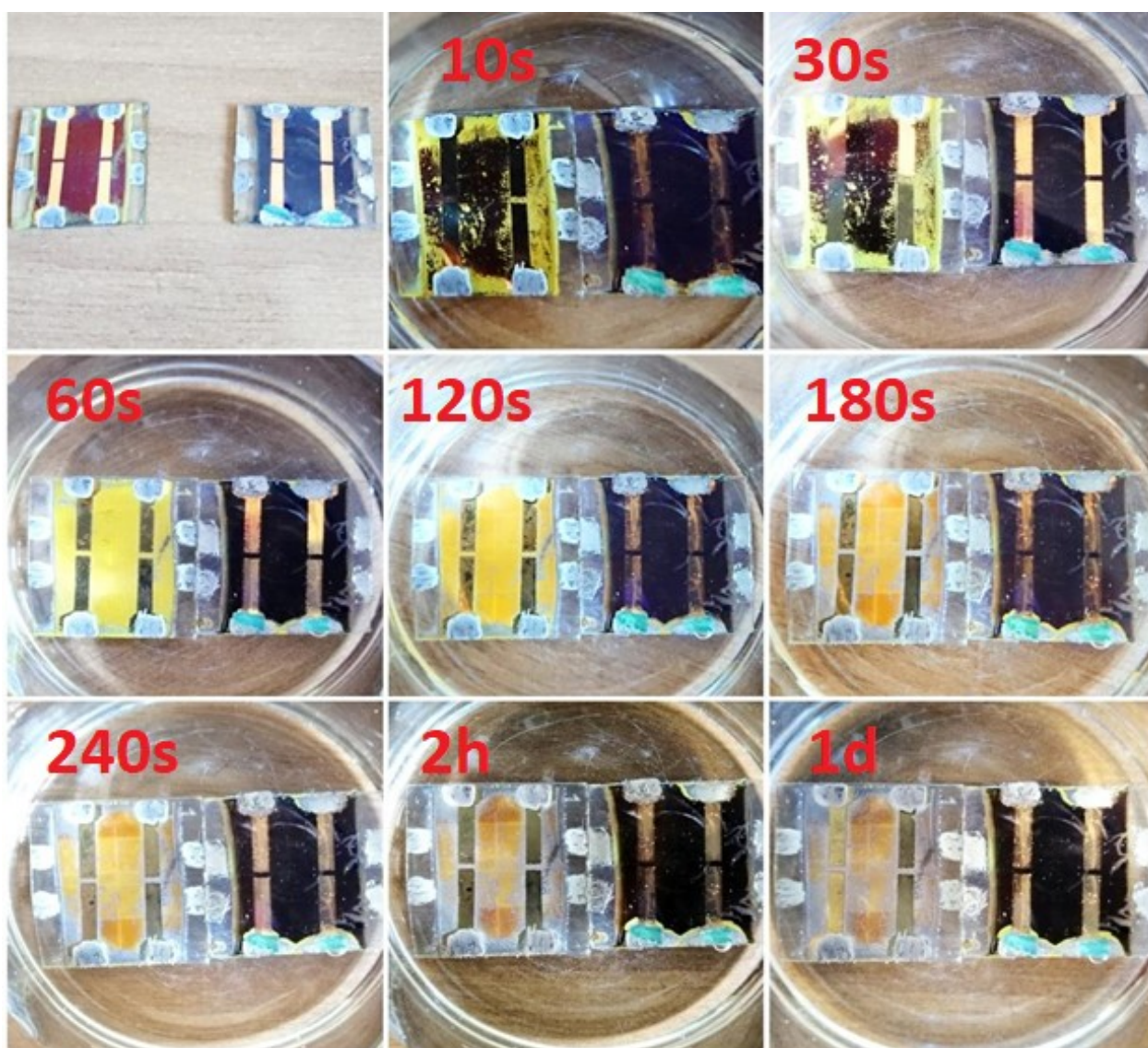


**Figure 6.** Dipping of unencapsulated (on the left) and PU23-encapsulated device (on the right) in deionized water for different amount of time. First photograph refers to samples stored for 2 days (*i.e.* polymerization time) in ambient condition.

## TABLES.

**Table 1.** Screening parameters for the thoughtful choice of the most suitable PU to be applied as encapsulant in Perovskite Solar Cells.

	PU11	PU12	PU13	PU21	PU22	PU23
Polyol formulation	1	1	1	2	2	2
Diisocyanate precursor	1	2	3	1	2	3
Viscosity at 25 °C [cP]	400	350	250	400	350	250
Hardness at 25 °C [Shore D]	78	34	24	75	32	22
First polymerization time [hours]	42	65	55	36	60	52
Decomposition Temperature [°C]	-	-	-	330.3	327.7	321.8
Residue at 400 °C [%]	-	-	-	4.6	4.4	4.3
Glass transition Temperature [°C]	-	-	-	41.2	13.3	8.5
Contact Angle [°]	-	-	-	101.5	101.8	102.7

## ASSOCIATED CONTENT

**Supporting Information.** Table S1: polymer-based encapsulant for PSCs. Figure S1-S3: Thermogravimetric Analyses of PU-based thermosetting resins. Figure S4-S6: Differential Scanning Calorimetry. Figure S7: Scheme of the deposition process. Figure S8: photograph of devices. Figure S9: Photoelectrochemical parameters of unencapsulated devices. Figure S10: Photoconversion efficiency as a function of ageing and polymerization time.

## AUTHOR INFORMATION

Corresponding Author

\*claudia.barolo@unito.it

\*Francesca.brunetti@uniroma2.it

## AUTHOR CONTRIBUTIONS

The manuscript was written through contributions of all authors. All authors have given approval to the final version of the manuscript.

## FUNDING SOURCES

This paper has been funded from the Italian Space Agency (ASI) project, PEROSKY Perovskite and other printable materials for energy application in space (no. 2018-1-R.0). S.C.H thanks Departamento del Huila's Scholarship Program No. 677 from Huila, Colombia for funding. This project (in the person of MB and CB) has received funding from the European Union's Horizon 2020 Research and Innovation Programme under grant agreement no. 826013 (IMPRESSIVE). BT, T.M.B. and FB would like to acknowledge the European Union's Horizon 2020 Research and Innovation Programme under grant agreement no. 763989 APOLO. FB and TMB would like to

acknowledge the European Union's Horizon 2020 Research and Innovation Programme under grant agreement no. 825213 WASP. This publication reflects only the author's views and the European Union is not liable for any use that may be made of the information contained therein.

## ACKNOWLEDGMENT

The authors gratefully acknowledge SE Special Engines S.r.l. for providing the PU precursors. M.B. acknowledge Dr. C. Atzori for technical support in XRD measurements and Dr. R. Fernandez de Luiz for profitable discussion on XRD data. C.B. and M.B. acknowledge A.Y. Bettozzi for support in PU characterization. Dr. I. Roppolo is thanked for the support in WVTR and OTR measurements. The authors acknowledge Ms. Giorgia Tradico for the realization of the ToC.

## REFERENCES

- (1) Jena, A. K.; Kulkarni, A.; Miyasaka, T. Halide Perovskite Photovoltaics: Background, Status, and Future Prospects. *Chem. Rev.* **2019**, *119* (5), 3036–3103. <https://doi.org/10.1021/acs.chemrev.8b00539>.
- (2) Nazeeruddin, M. K.; Baranoff, E.; Grätzel, M. Dye-Sensitized Solar Cells: A Brief Overview. *Sol. Energy* **2011**, *85* (6), 1172–1178. <https://doi.org/10.1016/j.solener.2011.01.018>.
- (3) Solanki, M. S.; Dangi, T.; Tak, P.; Sharma, S.; Ameta, R. Organic Photovoltaic Cells. *Sol. Energy Convers. Storage Photochem. Modes* **2015**, *10* (11), 55–84. <https://doi.org/10.1201/b19148>.

- (4) Dagar, J.; Castro-Hermosa, S.; Lucarelli, G.; Cacialli, F.; Brown, T. M. Highly Efficient Perovskite Solar Cells for Light Harvesting under Indoor Illumination via Solution Processed SnO<sub>2</sub>/MgO Composite Electron Transport Layers. *Nano Energy* **2018**, *49*, 290–299. <https://doi.org/10.1016/j.nanoen.2018.04.027>.
- (5) Kulkarni, S. A.; Mhaisalkar, S. G.; Mathews, N.; Boix, P. P. Perovskite Nanoparticles: Synthesis, Properties, and Novel Applications in Photovoltaics and LEDs. *Small Methods*. 2019, p 1800231. <https://doi.org/10.1002/smtd.201800231>.
- (6) Conings, B.; Drijkoningen, J.; Gauquelin, N.; Babayigit, A.; D'Haen, J.; D'Olieslaeger, L.; Ethirajan, A.; Verbeeck, J.; Manca, J.; Mosconi, E.; De Angelis, F.; Boyen, H. G. Intrinsic Thermal Instability of Methylammonium Lead Trihalide Perovskite. *Adv. Energy Mater.* **2015**, *5* (15), 1500477. <https://doi.org/10.1002/aenm.201500477>.
- (7) Berhe, T. A.; Su, W. N.; Chen, C. H.; Pan, C. J.; Cheng, J. H.; Chen, H. M.; Tsai, M. C.; Chen, L. Y.; Dubale, A. A.; Hwang, B. J. Organometal Halide Perovskite Solar Cells: Degradation and Stability. *Energy and Environmental Science*. 2016, pp 323–356. <https://doi.org/10.1039/c5ee02733k>.
- (8) Boyd, C. C.; Cheacharoen, R.; Leijtens, T.; McGehee, M. D. Understanding Degradation Mechanisms and Improving Stability of Perovskite Photovoltaics. *Chem. Rev.* **2019**, *119* (5), 3418–3451. <https://doi.org/10.1021/acs.chemrev.8b00336>.
- (9) Domanski, K.; Graetzel, M.; Tress, W. R. The Quest for Stability of Perovskite Solar Cells: Understanding Degradation, Improving Lifetimes and Towards Experimental Standards, Lausanne, EPFL, 2018. <https://doi.org/10.5075/epfl-thesis-8106>.

- (10) Aitola, K.; Domanski, K.; Correa-Baena, J. P.; Sveinbjörnsson, K.; Saliba, M.; Abate, A.; Grätzel, M.; Kauppinen, E.; Johansson, E. M. J.; Tress, W.; Hagfeldt, A.; Boschloo, G. High Temperature-Stable Perovskite Solar Cell Based on Low-Cost Carbon Nanotube Hole Contact. *Adv. Mater.* **2017**, *29* (17), 1606398. <https://doi.org/10.1002/adma.201606398>.
- (11) Jena, A. K.; Numata, Y.; Ikegami, M.; Miyasaka, T. Role of Spiro-OMeTAD in Performance Deterioration of Perovskite Solar Cells at High Temperature and Reuse of the Perovskite Films to Avoid Pb-Waste. *J. Mater. Chem. A* **2018**, *6* (5), 2219–2230. <https://doi.org/10.1039/C7TA07674F>.
- (12) Zhao, X.; Kim, H. S.; Seo, J. Y.; Park, N. G. Effect of Selective Contacts on the Thermal Stability of Perovskite Solar Cells. *ACS Appl. Mater. Interfaces* **2017**, *9* (8), 7148–7153. <https://doi.org/10.1021/acsami.6b15673>.
- (13) Domanski, K.; Correa-Baena, J.-P.; Mine, N.; Nazeeruddin, M. K.; Abate, A.; Saliba, M.; Tress, W.; Hagfeldt, A.; Grätzel, M. Not All That Glitters Is Gold: Metal-Migration-Induced Degradation in Perovskite Solar Cells. *ACS Nano* **2016**, *10* (6), 6306–6314. <https://doi.org/10.1021/acsnano.6b02613>.
- (14) Boyd, C. C.; Cheacharoen, R.; Bush, K. A.; Prasanna, R.; Leijtens, T.; McGehee, M. D. Barrier Design to Prevent Metal-Induced Degradation and Improve Thermal Stability in Perovskite Solar Cells. *ACS Energy Lett.* **2018**, *3* (7), 1772–1778. <https://doi.org/10.1021/acsenenergylett.8b00926>.
- (15) Jena, A. K.; Ikegami, M.; Miyasaka, T. Severe Morphological Deformation of Spiro-OMeTAD in (CH<sub>3</sub>NH<sub>3</sub>)PbI<sub>3</sub> Solar Cells at High Temperature. *ACS Energy Letters*. 2017,



- pp 1760–1761. <https://doi.org/10.1021/acsenergylett.7b00582>.
- (16) Domanski, K.; Alharbi, E. A.; Hagfeldt, A.; Grätzel, M.; Tress, W. Systematic Investigation of the Impact of Operation Conditions on the Degradation Behaviour of Perovskite Solar Cells. *Nat. Energy* **2018**, 3 (1), 61–67. <https://doi.org/10.1038/s41560-017-0060-5>.
  - (17) Castro-Hermosa, S.; Top, M.; Dagar, J.; Fahlteich, J.; Brown, T. M. Quantifying Performance of Permeation Barrier—Encapsulation Systems for Flexible and Glass-Based Electronics and Their Application to Perovskite Solar Cells. *Adv. Electron. Mater.* **2019**, 5 (10), 1800978. <https://doi.org/10.1002/aelm.201800978>.
  - (18) da Silva Sobrinho, A. S.; Latrèche, M.; Czeremuszkin, G.; Klemberg-Sapieha, J. E.; Wertheimer, M. R. Transparent Barrier Coatings on Polyethylene Terephthalate by Single- and Dual-Frequency Plasma-Enhanced Chemical Vapor Deposition. *J. Vac. Sci. Technol. A* **1998**, 16 (6), 3190–3198. <https://doi.org/10.1116/1.581519>.
  - (19) Li, X.; Tschumi, M.; Han, H.; Babkair, S. S.; Alzubaydi, R. A.; Ansari, A. A.; Habib, S. S.; Nazeeruddin, M. K.; Zakeeruddin, S. M.; Grätzel, M. Outdoor Performance and Stability under Elevated Temperatures and Long-Term Light Soaking of Triple-Layer Mesoporous Perovskite Photovoltaics. *Energy Technol.* **2015**, 3 (6), 551–555. <https://doi.org/10.1002/ente.201500045>.
  - (20) Burhan, M.; Shahzad, M. W.; Ng, K. C. *Concentrated Photovoltaic (CPV): From Deserts to Rooftops*; 2019; Vol. 70, pp 93–111. [https://doi.org/10.1007/978-3-030-05636-0\\_5](https://doi.org/10.1007/978-3-030-05636-0_5).
  - (21) Uddin, A.; Upama, M. B.; Yi, H.; Duan, L. Encapsulation of Organic and Perovskite Solar Cells: A Review. *Coatings*. 2019, p 65. <https://doi.org/10.3390/coatings9020065>.

- (22) Cheacharoen, R.; Boyd, C. C.; Burkhard, G. F.; Leijtens, T.; Raiford, J. A.; Bush, K. A.; Bent, S. F.; McGehee, M. D. Encapsulating Perovskite Solar Cells to Withstand Damp Heat and Thermal Cycling. *Sustain. Energy Fuels* **2018**, *2* (11), 2398–2406. <https://doi.org/10.1039/c8se00250a>.
- (23) Niu, G.; Guo, X.; Wang, L. Review of Recent Progress in Chemical Stability of Perovskite Solar Cells. *J. Mater. Chem. A* **2015**, *3* (17), 8970–8980. <https://doi.org/10.1039/c4ta04994b>.
- (24) Elkington, D.; Cooling, N.; Zhou, X. J.; Belcher, W. J.; Dastoor, P. C. Single-Step Annealing and Encapsulation for Organic Photovoltaics Using an Exothermically-Setting Encapsulant Material. *Sol. Energy Mater. Sol. Cells* **2014**, *124*, 75–78. <https://doi.org/10.1016/j.solmat.2014.01.039>.
- (25) Mariotti, N.; Bonomo, M.; Barolo, C. Emerging Photovoltaic Technologies and Eco-Design—Criticisms and Potential Improvements. In *Criticisms and Potential Improvements, Reliability and Ecological Aspects of Photovoltaic Modules*; Gok, A., Ed.; IntechOpen: London, 2020. <https://doi.org/10.5772/intechopen.88327>.
- (26) Kim, H. G.; Lee, J. G.; Kim, S. S. Self-Assembled Monolayers as a Defect Sealant of Al<sub>2</sub>O<sub>3</sub> Barrier Layers Grown by Atomic Layer Deposition. *Org. Electron.* **2018**, *52*, 98–102. <https://doi.org/10.1016/j.orgel.2017.10.004>.
- (27) Dameron, A. A.; Davidson, S. D.; Burton, B. B.; Carcia, P. F.; Scott McLean, R.; George, S. M. Gas Diffusion Barriers on Polymers Using Multilayers Fabricated by Al<sub>2</sub>O<sub>3</sub> and Rapid SiO<sub>2</sub> Atomic Layer Deposition. *J. Phys. Chem. C* **2008**, *112* (12), 4573–4580.

<https://doi.org/10.1021/jp076866+>.

- (28) Choi, E. Y.; Kim, J.; Lim, S.; Han, E.; Ho-Baillie, A. W. Y.; Park, N. Enhancing Stability for Organic-Inorganic Perovskite Solar Cells by Atomic Layer Deposited Al<sub>2</sub>O<sub>3</sub> Encapsulation. *Sol. Energy Mater. Sol. Cells* **2018**, *188*, 37–45. <https://doi.org/10.1016/j.solmat.2018.08.016>.
- (29) Reese, M. O.; Gevorgyan, S. A.; Jørgensen, M.; Bundgaard, E.; Kurtz, S. R.; Ginley, D. S.; Olson, D. C.; Lloyd, M. T.; Morvillo, P.; Katz, E. A.; Elschner, A.; Haillant, Olivier C.; Travis R.; Shrotriya, V.; Hermenau, M.; Riede, M.; Kirov, K. R. Trimmel, G.; Rath, T.; Inganäs, O.; Zhang, F.; Andersson, M.; Tvingstedt, K.; Lira-Cantu, M.; Laird, D.; McGuinness, C.; Gowrisanker, S.; Pannone, M.; Xiao, M.; Hauch, J.; Steim, R.; Delongchamp, D. M.; Rösch, R.; Hoppe, H.; Espinosa, N.; Urbina, A.; Yaman-Uzunoglu, G.; Bonekamp, J. B.; Van Breemen, A. J. J. M.; Girotto, C.; Voroshazi, E.; Krebs, F.C. Consensus Stability Testing Protocols for Organic Photovoltaic Materials and Devices. *Sol. Energy Mater. Sol. Cells* **2011**, *95* (5), 1253–1267. <https://doi.org/10.1016/j.solmat.2011.01.036>.
- (30) Yoo, S.; Lee, J.; Han, D.; Kim, H. Flexible Organic Solar Cells for Scalable, Low-Cost Photovoltaic Energy Conversion. In *Large Area and Flexible Electronics*; 2015; pp 439–468. <https://doi.org/10.1002/9783527679973.ch16>.
- (31) Duan, Y.; Wang, X.; Duan, Y. H.; Yang, Y. Q.; Chen, P.; Yang, D.; Sun, F. B.; Xue, K. W.; Hu, N.; Hou, J. W. High-Performance Barrier Using a Dual-Layer Inorganic/Organic Hybrid Thin-Film Encapsulation for Organic Light-Emitting Diodes. *Org. Electron.* **2014**, *15* (9), 1936–1941. <https://doi.org/10.1016/j.orgel.2014.05.001>.

- (32) Kim, N.; Graham, S.; Hwang, K. J. Enhancement of the Barrier Performance in Organic/Inorganic Multilayer Thin-Film Structures by Annealing of the Parylene Layer. *Mater. Res. Bull.* **2014**, *58*, 24–27. <https://doi.org/10.1016/j.materresbull.2014.03.022>.
- (33) Wang, R.; Mujahid, M.; Duan, Y.; Wang, Z. K.; Xue, J.; Yang, Y. A Review of Perovskites Solar Cell Stability. *Advanced Functional Materials*. 2019, p 1808843. <https://doi.org/10.1002/adfm.201808843>.
- (34) Wang, H.; Zhao, Y.; Wang, Z.; Liu, Y.; Zhao, Z.; Xu, G.; Han, T. H.; Lee, J. W.; Chen, C.; Bao, D.; Huang, Y.; Duana, Y.; Yang, Y. Hermetic Seal for Perovskite Solar Cells: An Improved Plasma Enhanced Atomic Layer Deposition Encapsulation. *Nano Energy* **2020**, *69*, 104375. <https://doi.org/10.1016/j.nanoen.2019.104375>.
- (35) Matteocci, F.; Cinà, L.; Lamanna, E.; Cacovich, S.; Divitini, G.; Midgley, P. A.; Ducati, C.; Di Carlo, A. Encapsulation for Long-Term Stability Enhancement of Perovskite Solar Cells. *Nano Energy* **2016**, *30*, 162–172. <https://doi.org/10.1016/j.nanoen.2016.09.041>.
- (36) Ramasamy, E.; Karthikeyan, V.; Rameshkumar, K.; Veerappan, G. Glass-to-Glass Encapsulation with Ultraviolet Light Curable Epoxy Edge Sealing for Stable Perovskite Solar Cells. *Mater. Lett.* **2019**, *250*, 51–54. <https://doi.org/10.1016/j.matlet.2019.04.082>.
- (37) Kim, N.; Potscavage, W. J.; Sundaramoorthi, A.; Henderson, C.; Kippelen, B.; Graham, S. A Correlation Study between Barrier Film Performance and Shelf Lifetime of Encapsulated Organic Solar Cells. *Sol. Energy Mater. Sol. Cells* **2012**, *101*, 140–146. <https://doi.org/10.1016/j.solmat.2012.02.002>.
- (38) Jarvis, K. L.; Evans, P. J.; Cooling, N. A.; Vaughan, B.; Habsuda, J.; Belcher, W. J.; Bilen,

- C.; Griffiths, G.; Dastoor, P. C.; Triani, G. Comparing Three Techniques to Determine the Water Vapour Transmission Rates of Polymers and Barrier Films. *Surfaces and Interfaces* **2017**, *9*, 182–188. <https://doi.org/10.1016/j.surfin.2017.09.009>.
- (39) Sonnenschein, M. F. *Polyurethanes: Science, Technology, Markets, and Trends*; 2014; Vol. 9781118737. <https://doi.org/10.1002/9781118901274>.
- (40) Huang, Z.; Hu, X.; Liu, C.; Tan, L.; Chen, Y. Nucleation and Crystallization Control via Polyurethane to Enhance the Bendability of Perovskite Solar Cells with Excellent Device Performance. *Adv. Funct. Mater.* **2017**, *27* (41), 1703061. <https://doi.org/10.1002/adfm.201703061>.
- (41) Kim, J.-E.; Kim, S.-S.; Zuo, C.; Gao, M.; Vak, D.; Kim, D.-Y. Humidity-Tolerant Roll-to-Roll Fabrication of Perovskite Solar Cells via Polymer-Additive-Assisted Hot Slot Die Deposition. *Adv. Funct. Mater.* **2019**, *29* (26), 1809194. <https://doi.org/10.1002/adfm.201809194>.
- (42) Carothers, W. H. Studies on Polymerization and Ring Formation. I. An Introduction to the General Theory of Condensation Polymers. *J. Am. Chem. Soc.* **1929**, *51* (8), 2548–2559. <https://doi.org/10.1021/ja01383a041>.
- (43) Motokucho, S.; Nakayama, Y.; Morikawa, H.; Nakatani, H. Environment-Friendly Chemical Recycling of Aliphatic Polyurethanes by Hydrolysis in a CO<sub>2</sub>-Water System. *J. Appl. Polym. Sci.* **2018**, *135* (8), 45897. <https://doi.org/10.1002/app.45897>.
- (44) Bella, F.; Griffini, G.; Correa-Baena, J. P.; Saracco, G.; Grätzel, M.; Hagfeldt, A.; Turri, S.; Gerbaldi, C. Improving Efficiency and Stability of Perovskite Solar Cells with Photocurable

- Fluoropolymers. *Science* **2016**, *354* (6309), 203–206.  
<https://doi.org/10.1126/science.aah4046>.
- (45) <https://polyurethane.americanchemistry.com/Polyurethane-Recycling/>.
- (46) Ying, W. Bin; Yu, Z.; Kim, D. H.; Lee, K. J.; Hu, H.; Liu, Y.; Kong, Z.; Wang, K.; Shang, J.; Zhang, R.; Zhu, J.; Li, R.W. Waterproof, Highly Tough, and Fast Self-Healing Polyurethane for Durable Electronic Skin. *ACS Appl. Mater. Interfaces* **2020**, *12* (9), 11072–11083. <https://doi.org/10.1021/acsami.0c00443>.
- (47) Wiles, A. A.; Bruckbauer, J.; Mohammed, N.; Cariello, M.; Cameron, J.; Findlay, N. J.; Taylor-Shaw, E.; Wallis, D. J.; Martin, R. W.; Skabara, P. J.; Cooke, G. A Poly(Urethane)-Encapsulated Benzo[2,3-D:6,7-d']Diimidazole Organic down-Converter for Green Hybrid LEDs. *Mater. Chem. Front.* **2020**, *4* (3), 1006–1012. <https://doi.org/10.1039/c9qm00771g>.
- (48) Fu, Z.; Xu, M.; Sheng, Y.; Yan, Z.; Meng, J.; Tong, C.; Li, D.; Wan, Z.; Ming, Y.; Mei, A.; Hu, Y.; Rong, Y.; Han, H. Encapsulation of Printable Mesoscopic Perovskite Solar Cells Enables High Temperature and Long-Term Outdoor Stability. *Adv. Funct. Mater.* **2019**, *29* (16), 1809129. <https://doi.org/10.1002/adfm.201809129>.
- (49) Yang, G.; Chen, C.; Yao, F.; Chen, Z.; Zhang, Q.; Zheng, X.; Ma, J.; Lei, H.; Qin, P.; Xiong, L.; Ke, W.; Li, G.; Yan, Y.; Fang, G. Effective Carrier-Concentration Tuning of SnO<sub>2</sub> Quantum Dot Electron-Selective Layers for High-Performance Planar Perovskite Solar Cells. *Adv. Mater.* **2018**, *30* (14). <https://doi.org/10.1002/adma.201706023>.
- (50) Ghoreishi, R.; Suppes, G. J. Chain Growth Polymerization Mechanism in Polyurethane-Forming Reactions. *RSC Adv.* **2015**, *5* (84), 68361–68368.

<https://doi.org/10.1039/c5ra10725c>.

- (51) Ahmad, D.; van den Boogaert, I.; Miller, J.; Presswell, R.; Jouhara, H. Hydrophilic and Hydrophobic Materials and Their Applications. *Energy Sources, Part A: Recovery, Utilization and Environmental Effects*. 2018, pp 2686–2725. <https://doi.org/10.1080/15567036.2018.1511642>.
- (52) Kim, N.; Graham, S. Development of Highly Flexible and Ultra-Low Permeation Rate Thin-Film Barrier Structure for Organic Electronics. In *Thin Solid Films*; 2013; Vol. 547, pp 57–62. <https://doi.org/10.1016/j.tsf.2013.05.007>.
- (53) Wang, H.; Wang, Z.; Yang, Z.; Xu, Y.; Ding, Y.; Tan, L.; Yi, C.; Zhang, Z.; Meng, K.; Chen, G.; Zhao, Y.; Luo, Y.; Zhang, X.; Hagfeldt, A.; Luo, J. Ligand-Modulated Excess PbI<sub>2</sub> Nanosheets for Highly Efficient and Stable Perovskite Solar Cells. *Adv. Mater.* **2020**, 32 (21), 2000865. <https://doi.org/10.1002/adma.202000865>.
- (54) Jacobsson, T. J.; Correa-Baena, J. P.; Halvani Anaraki, E.; Philippe, B.; Stranks, S. D.; Bouduban, M. E. F.; Tress, W.; Schenk, K.; Teuscher, J.; Moser, J. E.; Renmso, H.; Hagfeldt, A. Unreacted PbI<sub>2</sub> as a Double-Edged Sword for Enhancing the Performance of Perovskite Solar Cells. *J. Am. Chem. Soc.* **2016**, 138 (32), 10331–10343. <https://doi.org/10.1021/jacs.6b06320>.
- (55) Leguy, A. M. A.; Hu, Y.; Campoy-Quiles, M.; Alonso, M. I.; Weber, O. J.; Azarhoosh, P.; Van Schilfgaarde, M.; Weller, M. T.; Bein, T.; Nelson, J.; Docampo, P.; Barnes, P. R. F. Reversible Hydration of CH<sub>3</sub>NH<sub>3</sub>PbI<sub>3</sub> in Films, Single Crystals, and Solar Cells. *Chem. Mater.* **2015**, 27 (9), 3397–3407. <https://doi.org/10.1021/acs.chemmater.5b00660>.

- (56) Poli, I.; Eslava, S.; Cameron, P. Tetrabutylammonium Cations for Moisture-Resistant and Semitransparent Perovskite Solar Cells. *J. Mater. Chem. A* **2017**, *5* (42), 22325–22333. <https://doi.org/10.1039/c7ta06735f>.
- (57) Di Girolamo, D.; Dar, M. I.; Dini, D.; Gontrani, L.; Caminiti, R.; Mattoni, A.; Graetzel, M.; Meloni, S. Dual Effect of Humidity on Cesium Lead Bromide: Enhancement and Degradation of Perovskite Films. *J. Mater. Chem. A* **2019**, *7* (19), 12292–12302. <https://doi.org/10.1039/c9ta00715f>.
- (58) Zhang, M.; Wu, F.; Chi, D.; Shi, K.; Huang, S. High-Efficiency Perovskite Solar Cells with Poly(Vinylpyrrolidone)-Doped SnO<sub>2</sub> as an Electron Transport Layer. *Mater. Adv.* **2020**, *1* (4), 617–624. <https://doi.org/10.1039/d0ma00028k>.
- (59) Tyagi, B.; Lee, H. B.; Kumar, N.; Kang, J.-W. Double-Halide Composition Engineered SnO<sub>2</sub>-Triple Cation Perovskite Solar Cells Demonstrating Outstanding Performance and Stability. *ACS Appl. Energy Mater.* **2020**, in press. <https://doi.org/10.1021/acsaem.0c01214>.
- (60) Zhang, W.; Li, Y.; Liu, X.; Tang, D.; Li, X.; Yuan, X. Ethyl Acetate Green Antisolvent Process for High-Performance Planar Low-Temperature SnO<sub>2</sub>-Based Perovskite Solar Cells Made in Ambient Air. *Chem. Eng. J.* **2020**, *379*, 122298. <https://doi.org/10.1016/j.cej.2019.122298>.
- (61) Castro-Hermosa, S.; Lucarelli, G.; Top, M.; Fahland, M.; Fahlteich, J.; Brown, T. M. Perovskite Photovoltaics on Roll-To-Roll Coated Ultra-Thin Glass as Flexible High-Efficiency Indoor Power Generators. *Cell Reports Phys. Sci.* **2020**, *1* (5), 100045. <https://doi.org/10.1016/j.xcrp.2020.100045>.



- (62) Khenkin, M. V.; Katz, E. A.; Abate, A.; Bardizza, G.; Berry, J. J.; Brabec, C.; Brunetti, F.; Bulović, V.; Burlingame, Q.; Di Carlo, A.; Cheacharoen, R.; Cheng, Y. B.; Colsmann, A.; Cros, S.; Domanski, K.; Dusza, M.; Fell, C. J.; Forrest, S. R.; Galagan, Y.; Di Girolamo, D.; Grätzel, M.; Hagfeldt, A.; von Hauff, E.; Hoppe, H.; Kettle, J.; Köbler, H.; Leite, M. S.; Liu, S.; Loo, Y. L.; Luther, J. M.; Ma, C. Q.; Madsen, M.; Manceau, M.; Matheron, M.; McGehee, M.; Meitzner, R.; Nazeeruddin, M. K.; Nogueira, A. F.; Odabaşı, C.; Osherov, A.; Park, N. G.; Reese, M. O.; De Rossi, F.; Saliba, M.; Schubert, U. S.; Snaith, H. J.; Stranks, S. D.; Tress, W.; Troshin, P. A.; Turkovic, V.; Veenstra, S.; Visoly-Fisher, I.; Walsh, A.; Watson, T.; Xie, H.; Yıldırım, R.; Zakeeruddin, S. M.; Zhu, K.; Lira-Cantu, M. Consensus Statement for Stability Assessment and Reporting for Perovskite Photovoltaics Based on ISOS Procedures. *Nat. Energy* **2020**, *5* (1), 35–49. <https://doi.org/10.1038/s41560-019-0529-5>.
- (63) Verhoeven, V. W. A.; Padsalgikar, A. D.; Ganzeveld, K. J.; Janssen, L. P. B. M. A Kinetic Investigation of Polyurethane Polymerization for Reactive Extrusion Purposes. *J. Appl. Polym. Sci.* **2006**, *101* (1), 370–382. <https://doi.org/10.1002/app.23848>.
- (64) Nies, C.; Wehlack, C.; Ehbing, H.; Dijkstra, D. J.; Possart, W. Adhesive Interactions of Polyurethane Monomers with Native Metal Surfaces. *J. Adhes.* **2012**, *88* (8), 665–683. <https://doi.org/10.1080/00218464.2012.682865>.
- (65) Sherkar, T. S.; Momblona, C.; Gil-Escrig, L.; Ávila, J.; Sessolo, M.; Bolink, H. J.; Koster, L. J. A. Recombination in Perovskite Solar Cells: Significance of Grain Boundaries, Interface Traps, and Defect Ions. *ACS Energy Lett.* **2017**, *2* (5), 1214–1222. <https://doi.org/10.1021/acsenergylett.7b00236>.

- (66) Almora, O.; Zarazua, I.; Mas-Marza, E.; Mora-Sero, I.; Bisquert, J.; Garcia-Belmonte, G. Capacitive Dark Currents, Hysteresis, and Electrode Polarization in Lead Halide Perovskite Solar Cells. *J. Phys. Chem. Lett.* **2015**, *6* (9), 1645–1652. <https://doi.org/10.1021/acs.jpcclett.5b00480>.
- (67) Fei, C.; Wang, H. Age-Induced Recrystallization in Perovskite Solar Cells. *Org. Electron.* **2019**, *68*, 143–150. <https://doi.org/10.1016/j.orgel.2019.02.010>.
- (68) Liu, G.; Xi, X.; Chen, R.; Chen, L.; Chen, G. Oxygen Aging Time: A Dominant Step for Spiro-OMeTAD in Perovskite Solar Cells. *J. Renew. Sustain. Energy* **2018**, *10* (4), 043702. <https://doi.org/10.1063/1.5031167>.
- (69) Lee, Y.; Paek, S.; Cho, K. T.; Oveisi, E.; Gao, P.; Lee, S.; Park, J. S.; Zhang, Y.; Humphry-Baker, R.; Asiri, A. M.; Nazeeruddin, M. K. Enhanced Charge Collection with Passivation of the Tin Oxide Layer in Planar Perovskite Solar Cells. *J. Mater. Chem. A* **2017**, *5* (25), 12729–12734. <https://doi.org/10.1039/c7ta04128d>.
- (70) Dong, Q.; Liu, F.; Wong, M. K.; Tam, H. W.; Djurišić, A. B.; Ng, A.; Surya, C.; Chan, W. K.; Ng, A. M. C. Encapsulation of Perovskite Solar Cells for High Humidity Conditions. *ChemSusChem* **2016**, *9* (18), 2597–2603. <https://doi.org/10.1002/cssc.201600868>.

**SYNOPSIS.** Polyurethane-based thermosetting resins are implemented for the first time as effective oxygen and water barrier in planar n-i-p perovskite solar cells. Encapsulated devices retain more than 95% of initial efficiency when stored for 2500 hours under ambient light (400-

1000 lux) controlled humidity (28-65%) and temperature (18-30 °C). The implementation of the encapsulant positively influences the photostability of the perovskite layer.

